1 **Cell competition overcomes host tissue resistance to unleash tumour growth**

2 **in a *Drosophila* brain cancer model**

3

4

5

6

7 Marco Gualtieri[1,2], Saline Jabre[1], Damien Mornico[3], Maëlwenn Hamon[1], Cédric Maurange[4]

8 and Pauline Spéder[1]

9

10 1. Institut Pasteur, CNRS, UMR3738, Université Paris Cité, Equipe labellisée Fondation ARC

11 pour la Recherche contre le Cancer Paris, France.

12 2. Sorbonne Université, Collège Doctoral, ED515, Paris, France.

13 3. Hub de Bioinformatique et Biostatistique - Département Biologie Computationnelle, Institut

14 Pasteur, USR 3756 CNRS, Paris, France.

15 4. Aix Marseille University, CNRS, IBDM, Equipe labellisée Ligue Contre le Cancer, Marseille

16 13009, France

17

18

19 ***Corresponding author:**

20 Pauline Spéder, PhD
21 Department of Developmental and Stem Cell Biology
22 Institut Pasteur/CNRS UMR3738
23 25 rue du Docteur Roux
24 75015 PARIS
25 E-mail : pauline.speder@pasteur.fr
26 Phone: + 33 1 45 68 89 78

1   **Abstract**

2   Primary tumours of the central nervous system are extremely aggressive and often incurable.

3   While tumours are known to interact with their microenvironment, how the interplay between

4   tumour cells and the host tissue controls tumour progression remains elusive. We addressed

5   this question in a *Drosophila* model of cancer stem cell-driven tumour which originates during

6   development and grows extensively within a network of cortex glia cells (CG) through

7   adulthood. We found that tumour growth induces progressive remodeling of the CG network

8   and leads to CG apoptosis through cancer stem cell-driven competition, a process which in turn

9   unleashes tumour growth. Notably, preventing CG death reduces tumour growth, revealing a

10   resistance capacity within the CG. Transcriptional profiling of CG cells at different stages

11   revealed a biphasic response, featuring an early specific signature followed by a later collapse

12   of essential cellular functions and pathways, including the conserved JNK pathway. JNK

13   signalling in CG normally plays a neuroprotective role and initially hinders tumour progression,

14   providing resistance. However, its subsequent downregulation eventually brings the collapse

15   of the host tissue, ultimately curbing tumour growth. This study uncovers a dynamic and

16   complex interplay between host tissue resistance and tumour-driven competition, which shapes

17   tumour progression.

Introduction

Primary tumours of the central nervous system (CNS) are extremely aggressive tumours which originate from and develop within the brain or spinal cord (*1*, *2*). They are still extraordinarily difficult to treat despite combined surgery, chemotherapy and radiotherapy, owing to their infiltrating nature challenging resection and to their place of origin, shielded behind strong cellular barriers and made of poorly replaceable cells. Survivors are left with important neurological sequelae and a degraded quality of life, from the tumour and/or the treatments. Tumour recurrence is also high. Another specificity of CNS tumours is their high incidence in children, accounting for 26% of new cancer cases versus 1.5% in adults (*3*) and making them the leading cause of cancer mortality during childhood. In contrast to adult tumours, pediatric tumours do not seem to accumulate multiple oncogenic mutations, while sharing highly proliferating and invasive properties (*4*).

CNS tumours originate from and are maintained by a restricted number of highly proliferative cells at the apex of the tumour cellular hierarchy. These cells, identified in several primary CNS tumours (*5–9*), are coined cancer stem cells (CSCs) and share many features of neural stem cells (NSCs), the multipotent progenitors of the CNS, whose transformation can lead to cancer development (reviewed in (*10–13*)). CSCs display NSC molecular markers, exhibit self-renewal potential and can birth differentiated progeny, while supporting the malignant tumour population through uncontrolled amplification. Developmental signalling pathways present in NSCs also re-emerge in CSCs to promote growth and invasiveness (*13*, *14*). CSCs are at the apex of the tumour cellular hierarchy, can re-initiate the tumour (*15*) and are proposed to resist current treatments, supporting cancer recurrence (*16*). CSC properties are increasingly linked to tumour growth and multi-scale complexity (competition, composition, invasiveness) (reviewed in (*10*, *14*, *17*)).

While tumour growth is fueled by the intrinsic proliferative ability of CSCs, it is now known that it can be dramatically influenced by extrinsic factors. Tumours indeed develop within, both with and against, the host tissue. The tumour microenvironment (TME) builds from the host components in vicinity to the tumour, and evolves over time, resulting from the progressive remodelling of the host tissue as well as from the contribution of CSC-produced cells. The interplay between tumour cells and the host tissue/TME is complex and multifaceted, and appears as a crucial driver of cancer progression (*18*, *19*). In CNS tumours, the host tissue, and thus the TME, is particularly intricate and made of highly diverse cellular components of

3

33 various origins, including neurons, glial cells, the blood-brain barrier and resident immune cells
34 (*20–22*).

35 Hijacking and rewiring of host cell functions by tumour cells have been well documented across
36 various cancer types, including CNS tumours, to support tumour progression by conferring
37 metabolic and immune advantages (*23, 24*). For instance, cross-talk between CSCs and
38 endothelial cells increases angiogenesis and accelerates CSCs' self-renewing capacity (*25*).
39 Tumour cells can actually set up connected networks between themselves or with host cells, a
40 property linked to tumour amplification and resistance to treatment (*26*). Moreover, neuron-
41 tumour interactions influence tumourigenesis at multiple steps and through diverse mechanisms
42 (reviewed in (*27, 28*)), including direct interaction through synapses (*29*) and coopting neuronal
43 migration (*26*). Glial cells, namely oligodendrocytes and astrocytes, are also part to the TME,
44 yet their interactions with tumour cells are still poorly characterized (reviewed in (*30, 31*)).
45 Tumour reactive-astrocytes promote glioma invasion through different factors (*31–34*).
46 Interestingly, in early stages, astrocytes seem to exert anti-tumour, cytotoxic effects before
47 becoming reactive, highlighting a dynamic interplay between the glial TME and tumour cells
48 (*35*). Despite growing attention to the role of the host tissue in oncogenesis, and evidence that
49 their properties are remodelled in cancer (*36, 37*), the contribution of glial cells to tumour
50 progression is still little understood.

51 Tumours can also reshape the TME by removing cells and have been proposed to use cell
52 competition to create physical and functional space for invasion (*38*). Cell competition has been
53 defined as a context-dependent process where one cell population ("winner cells") induces the
54 apoptosis of another ("looser cells"), leading to its elimination (*39*). This mechanism is thought
55 to support the proliferation of rapid-growing cells (known as super-competitors) by removing
56 and replacing neighbouring healthy cells. As such, this concept, originally investigated in
57 development and discovered in *Drosophila* epithelia (*40, 41*), has important implications for
58 cancer. A number of studies in epithelial tumours have now shown that tumour cells can kill
59 their neighbouring cells, either less fit tumour clones (thus shaping tumour clonality) or healthy
60 host cells (*42–46*), to boost their growth (reviewed in (*47–49*). Whether similar mechanisms
61 operate in the non-epithelial CNS tumours remain poorly characterized. Clonal competition
62 happens in glioblastoma, influencing tumour genetic composition (*50*). Moreover, CNS
63 tumours grow in a dense tissue with strong boundaries, creating solid stress which induces
64 neuronal death (*51*). High levels of cell death are detected across tumours and linked to poor
65 prognosis, with increasing evidence showing that dying cells positively affect tumour cells by

4

66   releasing beneficial factors (*52, 53*). However, while cell death regulation in tumour cells has

67   been extensively studied, given its potential for therapeutic targeting and its role in tumour

68   resistance (*54, 55*), the extent and function of cell death in the different host cells of the CNS,

69   and whether their sensitivities change in tumour conditions, remain poorly known (*56*). In

70   particular, whether *bona fidae* cell competition between cancer cells and the host tissue happens

71   in CNS tumours, and its relevance for the pathology, is not known.

72   Here, we used a *Drosophila* model of CNS tumour of developmental origin to decipher the

73   dynamics between the host tissue, specifically glial cells, and tumour progression. Aggressive,

74   CSC-driven tumours can be induced from transformed NSCs during the developing larval

75   stage, resulting in fast-growing tumours in adults. During normal development, Type I NSCs,

76   the most prominent NSC subtype in the fly CNS outside of the visual system, divide

77   asymmetrically to self-renew while generating an intermediate progenitor cell called ganglion

78   mother cell (GMC), which divides once more to produce two neurons or glial cells (**Fig. 1A**,

79   left panel) (*57*). Individual NSCs can be dysregulated in a cell-autonomous fashion to generate

80   tumours (*58, 59*). In particular, the loss of the Prox-related homeobox transcription factor

81   Prospero (Pros) produces GMCs which fail to differentiate and revert to a stem cell-like state

82   (*60*) (**Fig. 1A**, right panel). Each *pros⁻* NSC gives rise to a clonal tumour lineage mainly

83   composed of NSC-like cells, which amplify at the expense of normal neuronal output and which

84   persist and develop in the adult stage of the fly (**Fig. 1B-C**). To form tumours, *pros⁻* NSCs must

85   be induced during an early developmental window when the temporal factors Chinmo and Imp

86   are expressed (**Fig. 1A**, insert) (*61*). These *chinmo⁺ Imp⁺ pros⁻* NSCs have high proliferative

87   potential and persist indefinitely in the tumour, acting as self-renewing CSCs (*62*). They can

88   also generate more restricted *Syp⁺ pros⁻* progenitors in which *chinmo* and *Imp* are silenced

89   following the emergence of the RNA-binding protein Syp, leading to limited proliferative

90   capacity. Together, these populations form a heterogeneous, hierarchically organized tumour

91   with *Chinmo⁺ Imp⁺* CSCs at the apex (*62*) (**Fig. 1A**). Chinmo and Imp are reminiscent of

92   oncofetal genes, whose expression is normally restricted to embryonic/fetal stages and

93   reactivated in tumours. They appear to promote tumour growth by boosting cell metabolism

94   and self-renewal. These hierarchical CSC-driven tumours, induced during developmental

95   stages by the inactivation of a single gene, through co-option of developmental programs, offer

96   a simplified yet relevant model for studying pediatric tumour progression (*59, 61–63*).

97   These *pros⁻* CSC-driven tumours develop within a host tissue made of diverse cell types making

98   up the NSC niche (*64*), including the NSCs themselves, neurons, multiple glial subtypes (*65*)

5

99   and a blood-brain barrier (*66*) (**Fig. 1D-E**). The blood-brain barrier and glia provide lifelong

100 trophic support and regulatory inputs to NSCs and neurons. In particular, the cortex glia (CG)

101 form a highly connected membrane meshwork (*67–71*), infiltrating in-between individual NSC

102 lineages and neurons. The CG support and protect NSCs (*72–75*) and are essential for neuronal

103 positioning and survival (*67, 69, 76–78*). In the adult, the CG network exists around neurons

104 (**Fig. 1F-G**) and support their functions, such as sleep regulation (*79, 80*). Notably, the CG

105 structure, composed of interconnected cells which communicate and maintain close contact

106 with neurons, resembles the astrocytic networks found throughout the brain (*81*). Moreover,

107 CG interface with the blood-brain barrier, akin to the mammalian *glia limitans*, another reticular

108 structure made by astrocytic endfeet (*82*).

109 Here, we found that CG cells initially remodel their morphology to infiltrate the tumour, and

110 provide resistance to tumour growth. However CSC-mediated cell competition takes place and

111 results in the elimination of CG cells by apoptosis, a phenomenon which boosts tumour growth.

112 This biphasic TME remodelling is mirrored by transcriptional changes in CG cells,

113 characterized by an early specific signature followed by the collapse of core cell functions.

114 Amongst these changes, the downregulation in the CG of the normally active and

115 neuroprotective JNK pathway first helps tumour growth but later hinders it, a shift coinciding

116 with neuronal loss and overall tissue breakdown, and implying that JNK morphes from an anti-

117 to a pro-tumour role during the course of the tumour. These findings highlight the complexity

118 of tumour and host tissue interactions, and identify both cell competition and glial cells as

119 crucial players in CNS tumours.

1 **RESULTS**

2 **Cortex glia architecture is remodelled during tumour progression**

3 We used the UAS/GAL4 system to knockdown *pros* by driving a specific RNAi under the

4 genetic control of a Paired-box transcription factor Pox-Neuro (*poxn*) enhancer that is active in

5 only six Type I NSCs in the larval ventral nerve cord (VNC) (*83*) This system allows the

6 generation of six trackable tumours (hereafter referred to as *pros^poxn* tumours) in stereotyped

7 locations in the larval VNC (**Fig. 1B**) (*61*). Their cancer stem and progenitor cell population

8 (herein called CSPC), which makes most of the tumour bulk, can be marked with NSC

9 determinants such as the transcription factor Deadpan (Dpn) (**Fig. 1A**, insert). These *pros^poxn*

10 tumours grow from larval stages. A large part of CSPCs differentiate during metamorphosis, in

11 response to hormonal pulses, but a fraction persists in adult. From adult eclosion (day 0), the

12 persisting fraction of CSPCs continues to overproliferate, covering the entire VNC after a few

13 days, further invading the central brain, and ultimately killing the fly around days 10-12 (**Fig.**

14 **1B-C** and (*61*)).

15 To understand the interplay between CG cells and tumour progression, we first assessed their

16 morphology. During normal development, NSC lineages are found embedded in a membranous

17 chamber made by the CG (**Fig. 1D-E**), a grid-type pattern maintained by a balance of timely

18 set-up differential adhesions (*78*). This rule of whole lineage encasing stops when neurons

19 mature, and become individually enwrapped (*68, 78*). Previous work also showed that NSC-

20 derived tumours of different origins, induced in early developmental stages, stay confined

21 within a continuous CG enclosure during their growth at larval stage (*78*). Using the *Nrv2::GFP*

22 knock-in line to visualize the CG membranes and Dpn staining to detect the CSPCs, we found

23 that each of the six *pros^poxn* tumours similarly stayed contained inside CG chambers during

24 larval stages (**Fig. 1H and S1A**, L3 larval stage), with the tumour clones not merging with each

25 other. The individual tumours were also devoided of internal CG membrane.

26 We wondered whether such embedding was maintained during tumour progression in

27 adulthood and how effectively CG coped with the dramatic tumour growth. We found that, in

28 most VNCs, individual *pros^poxn* tumours were not no longer distinguishable by day 1, and we

29 rather observed one tumour mass spread throughout the whole VNC and infiltrated by

30 discontinuous CG membranes (**Fig. 1H and S1A**, Days 1, 3, 6 and 9). This was accompanied

31 by a progressive remodeling of the CG structure along tumour progression, displaying altered

32 membrane morphology and eventually losing its seemingly continuous network organization.

33 Quantifying the ratio between CG membrane and tumour volumes revealed an overall decrease

7

34   along tumour progression (**Fig. 1G**). Notably, neurons continued to be individually encased by

35   CG membranes, even the rare ones within the tumour mass (**Fig. 1H**, white arrowheads).

36   While the CG structure was disorganised, making individual tumours undiscernible, it remained

37   to be addressed whether the six *pros^{poxn}* tumours were meeting each other and truly merging or

38   whether they stayed separated from each other by CG membranes. To distinguish the original

39   six tumour clusters in the adult, we took advantage of a multicolour clonal labelling technique,

40   Raeppli (*84*), in which the stochastic expression of one out of four fluorophores, targeted to the

41   nucleus by a nuclear localization sequence (NLS-Raeppli), can be restricted to Poxn$^+$ NSC

42   lineages through the use of the GAL4/UAS system. Induction is done at larval stage to label

43   the Poxn$^+$ NSCs from which the tumours originate from (**Fig. 1J**). Ultimately, in the tumour

44   condition, each of the six initial NSCs generates a tumour clone stably marked by one out of

45   the four possible fluorophores (**Fig. 1K** and **S1B**, Larval stage) and which can be tracked

46   throughout adult stage (**Fig. S1C**). First, we found that tumour clones do not seem to mingle,

47   but rather stay on their own, as a compact group of same colour cells (**Fig. 1K** and **S1B**, days

48   1 and 6), a behaviour similar to what was observed for these and other tumours in larval stages.

49   Focusing on the zone between two clones, we observed that CG membranes, labelled by

50   Nrv2::GFP, were still present between different *pros^{poxn}* tumours at later stages (days 3 and 6,

51   white arrows), suggesting that the CG still maintain its singular embedding of clonal lineages.

52   We however noticed the presence of many infiltrating CG membranes within individual *pros^{poxn}*

53   tumours (**Fig. 1K** and **Fig. S1D**, pink arrowheads), confirming our previous observation.

54   Altogether, these data suggest that during tumour progression, CG maintain the developmental

55   principle of encasing whole lineages for undifferentiated cells and encasing individual cells for

56   neurons. Yet, CG organisation remodels around tumours, with the early formation of internal

57   membrane projections infiltrating in-between CSPCs and whose density within the tumour

58   decreases overtime.

59   **Cancer stem cell-driven cell competition induces close-by cortex glia apoptosis**

60   The dramatic expansion in volume of *pros^{poxn}* tumours, together with CG remodelling, made us

61   wonder how they could push against the host tissue and, specifically, whether it was at the

62   expense of neurons and glia.

63   We first asked whether host cells were displaced or lost during tumour progression. We stained

64   tumour and control CNSs at different stages of tumour progression (3 and 6 days old adults)

65   with a marker for glial (transcription factor Repo) and neuronal (transcription factor ElaV)

8

66   fates. We first found that both glia and neuron nuclei appear mislocalized in the tumour VNC

67   compared to control (**Fig. 2A**), exhibiting patterns ranging from strewn to clumped throughout

68   tumour progression. We also noticed a qualitative decrease in the overall glial staining. We then

69   quantified the neuronal and glial populations using the ElaV and Repo markers. Since

70   individual neuronal signal was challenging to segment (due to high neuronal density), we

71   decided to use the total volume of nuclei over time as a proxy volume of the cell population for

72   each cell type (see Methods). Thus, from now on, neuronal or glial volume will refer to total

73   nuclei volume for the respective population. Quantification of neuronal volume showed no

74   significant difference between control and tumour condition (**Fig. 2B**). In contrast, glial volume

75   was significantly reduced in tumour conditions compared to controls, at both day 3 and day 6

76   (**Fig. 2C**). These results show that tumour progression leads to glial, but not neuronal loss,

77   suggesting that neurons are more resistant to tumour progression or/and that the tumour

78   primarily affects glial cells.

79   Glial loss in tumour conditions could result either from disruption of physiological,

80   programmed proliferation or from increased cell death. While the former explanation appeared

81   less likely, as glial cells are deemed post-mitotic, it remained to be ruled out. Moreover, whether

82   the glial loss could be allocated, at least in part, to the CG, was also left to be shown. To address

83   both points, we specifically labelled CG nuclei using a *His::mCherry* transgene under the

84   control of a CG-specific promoter (*cyp4g15*) (**Fig. 2D**), and quantified both the number and

85   individual volume of CG nuclei at days 1, 3 and 6 in normal and tumour condition (**Fig. 2E-F**).

86   Unexpectedly, we first found that in normal situation, CG displayed stereotyped and timed

87   changes in nuclei number and individual nuclear volume over time, suggestive of some

88   proliferative behaviour. CG nuclei number stayed at similar level between day 1 and day 3 but

89   showed a distinct increase at day 6 (**Fig. 2E**), while CG individual nuclear volume increased

90   between day 1 and day 3 then tended towards decrease at day 6 (**Fig. 2F**). Considering these

91   two parameters together, and in light of CG known proliferative behaviour in larval stage (*70*),

92   we propose that adult CG first undergo an endoreplicative phase, between day 1 and day 3,

93   followed by nuclear division between day 3 and day 6. These results suggest that glia

94   development continues beyond the larval stage and proceeds into early adulthood, following a

95   timed pattern of proliferation.

96   These finding suggested that the decrease in glial volume observed during tumour progression

97   could result from the loss of CG proliferation occurring at day 6. However, quantification of

98   CG nuclei in tumour conditions at day 6 (**Fig. 2E**) revealed a greater loss than expected from

99   proliferation arrest alone, indicating that additional mechanisms contribute to glial loss.
100   Similarly, CG individual nuclear volume in tumour conditions was reduced compared to
101   controls, suggesting a loss of nuclear content (**Fig. 2F**).

102   Altogether, these data show that during tumour progression CG nuclei decrease in volume and
103   in number through mechanisms beyond sole proliferation arrest.

104   A straightforward explanation would be that glia undergo apoptosis. To test this hypothesis, we
105   took advantage of an apoptotic sensor (*85*), in which the GC3Ai domain (caspase 3-like
106   proteases activity indicator) is fused to an inactive GFP. Upon caspase-3 mediated cleavage,
107   the sensor undergoes a conformational change, allowing GFP fluorescence. We counted all
108   GFP-positive cells as a readout of caspase activation (and further likely apoptosis) during
109   tumour progression compared to control, at days 1, 3 and 6 of adulthood. We found a significant
110   increase in GC3Ai$^+$ cells in the tumour context at all timepoints (**Fig. 3. A-B**). We then analysed
111   the spatial distribution of the GC3Ai$^+$ cells relative to the tumour and found that the majority
112   of events occurred in close proximity of the tumour (distance of one to two cells), either at the
113   tumour edge or embedded within the tumour, with few GC3Ai$^+$ cells located as far as 13 cells
114   away (**Fig. 3C-D**). The more the tumour progressed, the more the distance was mostly shifted
115   to one cell, likely because the expanding tumour occupies most of the tissue, bringing non
116   tumour-related apoptotic events into closer proximity. These findings demonstrate that caspase
117   activation predominantly occurs in cells in close vicinity of the tumour. Co-staining for cell fate
118   markers for glia (Repo) and neuron (ElaV) revealed that most GC3Ai$^+$ cells were negative for
119   these markers (**Fig. 3C**), possibly because dying cells downregulate their identity marker before
120   expression of the effector caspase.

121   Given the decrease in glial volume and CG nuclei number and individual volume, together with
122   the increase in caspase activation seen in the TME under tumour condition, we propose that
123   glial cells, including CG cells, undergo apoptosis during tumour progression.

124   We next sought to assess the relationship between tumour growth and degree of glial loss. To
125   address this, we used the double loss of *pros* and *Syp*, a condition known to produce bigger
126   tumours than *pros* knockdown alone, being nearly exclusively constituted of *Chinmo$^+$ Imp$^+$*
127   *pros$^-$* CSCs (*62*) (**Fig. 1A and 3E**). We indeed recapitulated these findings, with *Syp^{RNAi} pros^{poxn}*
128   tumours displaying from day 1 more than a twofold increase in tumour volume, followed by an
129   even bigger difference at day 3 (**Fig. S2A-B**). Measuring glial volume (Repo) per VNC showed
130   a more pronounced decrease in *Syp pros^{poxn}* tumours compared to *pros^{poxn}* tumours, at both
131   timepoints (**Fig. S2C**). In line with this finding, quantifying the number of apoptotic cells using

132   cleaved effector caspase (Dcp-1) staining revealed an increase in Syp^{RNAi} $pros^{poxn}$ tumours
133   compared to $pros^{poxn}$ tumours (**Fig. S2D**). Of note, total neuronal volume (ElaV) per VNC did
134   not significantly change in Syp^{RNAi} $pros^{poxn}$ tumours compared to $pros^{poxn}$ tumours, although
135   there was a slight tendency towards a decrease (**Fig. S2E**).

136   These data indicate that glial loss is enhanced in the fast-growing Syp^{RNAi} $pros^{poxn}$ tumours. We
137   further tested the correlation between tumour and glial volumes in these two tumour conditions.
138   Strikingly, we found no significant correlation between tumour and glial volumes in $pros^{poxn}$
139   tumours, whereas these two parameters were negatively correlated in Syp^{RNAi} $pros^{poxn}$ tumours
140   (**Fig. 3F**). Similarly, when assessing the relationship between tumour volume and the level of
141   apoptosis (as measured by the number of Dcp-1$^+$ cells), we found no significant correlation in
142   $pros^{poxn}$ tumours, but a positive correlation emerged in Syp^{RNAi} $pros^{poxn}$ tumours (**Fig. 3G**). This
143   shows that glial apoptosis and loss do not occur as direct, linear consequences of tumour
144   growth, and also that they can be shifted to such relationship in Syp^{RNAi} $pros^{poxn}$ tumours.
145   Notably, Syp^{RNAi} $pros^{poxn}$ tumours differ in composition from $pros^{poxn}$ tumours, as they are
146   highly enriched in CSCs (from about 20% to more than 90% of total tumour volume), which in
147   turn causes accelerated tumour growth (*62*). Within this context, our findings suggest that CSC
148   concentration is a critical factor influencing the extent of glial loss, and that CSCs are primary
149   drivers of glial apoptosis.

150   Altogether, our findings show that CG cells undergo apoptosis in response to tumour growth
151   and propose a cell competition phenomenon whereby tumour cells, and especially CSCs,
152   eliminate their neighbouring glial cells.

153   **Manipulation of cortex glia apoptosis reveals both its requirement for tumour progression**
154   **and an intrinsic ability for resistance of the host tissue**

155   We decided to investigate the impact of CG apoptosis on tumour growth.
156   We first assessed the consequence of inducing apoptosis in CG in a precocious manner, at the
157   beginning of adulthood and throughout the whole CG population. We took advantage of the QF
158   binary system to drive the pro-apoptotic *reaper* gene in the CG (*cyp > reaper*) while inducing
159   tumour formation through the GAL4/UAS system, as done previously (*poxn > pros^{RNAi}*,
160   *pros^{poxn}* tumours) (**Fig. 4A**). The timing of induction was controlled using a heat-inducible
161   cassette (see Methods) to trigger glial apoptosis from adult eclosion (day 0). The increase in
162   cell death events was verified by staining for Dcp-1 at day 6 (**Fig. 4B**). Although it did not reach
163   statistical significance at this timepoint, we observed an upward trend, with some strongly
164   stained VNCs. We then measured the tumour volume overtime by quantifying the Dpn$^+$ cells.

11

165   Remarkably, inducing early and widespread CG apoptosis resulted in a significant increase in

166   tumour volume both at day 3 and day 6 compared to a control tumour condition (**Fig. 4C**).

167   We then wondered whether preventing apoptosis in glia during tumour progression would have

168   the opposite effect of slowing down tumour growth. To test this, we expressed the anti-

169   apoptotic baculovirus protein, p35 in the CG (*cyp > p35*), from adult eclosion (again relying on

170   the QF system and heat induction, see Methods) and throughout tumour progression (**Fig. 4D**).

171   We first checked whether p35 expression rescued the glial loss witnessed previously. We

172   decided to assess day 6 to ensure that effects of p35 expression could be detected after apoptosis

173   should have been ongoing for some time. We found that glial volume was significantly

174   increased in the tumour condition plus p35 expression in the CG (*poxn > pros^{RNAi}, cyp > p35*)

175   compared to a control tumour condition (*poxn > pros^{RNAi}, pros^{poxn}* tumours) (**Fig. 4E**). This

176   result confirmed both the effectiveness of p35 induction and our conclusion that CG undergo

177   apoptosis during tumour growth. However, the rescue was only partial when compared to the

178   glial volume measured in non tumour condition (see **Fig. 2C**). It could imply that either p35

179   expression did not rescue all apoptotic events in the CG or it rescued most but resulted in

180   smaller CG cells (*86*). Alternatively, other glial subtypes may die during tumour growth, or the

181   observed glial loss might also reflect altered proliferation rather than solely apoptosis. We then

182   measured tumour volume under p35 expression in the CG and strikingly we found that at day

183   6 it was significantly decreased compared to the tumour without p35 expression (**Fig. 4F**).

184   Altogether these results show that tumour-induced CG apoptosis promotes tumour growth in

185   the host tissue. They also reveal that the CG have the potential to impair tumour progression

186   when they are maintained in the TME.

187   **Temporal analysis of cortex glia transcriptome reveals a biphasic response to tumour**

188   **progression**

189   These results highlighted a potential tug-of-war between tumour cells and CG cells, where

190   tumour cells, and in particular CSCs, induce, directly or indirectly, CG cell death, while CG

191   cells exhibit some resistance to tumour progression. To better characterize the behaviour of the

192   CG cells and potentially identify molecular players causing their death or supporting their

193   resistance ability, we determined the transcriptional changes taking place in the CG along

194   tumour growth. We used the Targeted DamID Pol II (TaDa-Pol II) method (*87, 88*), which

195   allows the tracking of gene expression in specific cell types for given time windows, without

196   having to isolate those cells. This technique uses an enzyme called DNA adenine

197   methyltransferase (Dam), which adds methyl groups to genomic GATC sequences. Fusing Dam

12

198   with a core subunit of RNA polymerase II (Pol II) results in the methylation of the sequences
199   nearby the polymerase II binding sites, which are mapped to identify paused and active
200   transcription. Controlling its expression by genetic binary systems enables time- and cell
201   population-specific methylation signals. In our case, we placed TaDa-Pol II under the control
202   of the QF system, using a heat-inducible CG-specific driver, while inducing $pros^{poxn}$ tumours
203   through the GAL4/UAS system (**Fig. S3A**), similarly to the *reaper* and *p35* strategy.

204   We performed TaDa-Pol II at day 1 and day 6 of adulthood, for both $pros^{poxn}$ tumour and non-
205   tumour control conditions (**Fig. 5A**). Statistical cross-comparison of the four datasets allowed
206   us to identify gene expression changes in CG between tumour and control conditions over time
207   (**Fig. 5B** ; **Dataset S1**). First, we observed a specific response of the CG at day 1 of tumour
208   progression, characterized by a similar number of up- and down-regulated genes. At day 6
209   however CG display a prominent decrease in gene expression, both compared to the non-
210   tumour condition at day 6 and to the tumour condition at day 1. KEGG pathway enrichment
211   confirmed this biphasic behaviour (**Fig. 5C**; **Dataset S2**). A specific molecular signature of CG
212   cells was revealed at day 1 in tumour context, characterized by an immunity (orange bar) and
213   a lipid metabolism (red bar) components. At day 6 however, most of the downregulated genes
214   belonged to core cellular and metabolic pathways, including oxidative phosphorylation,
215   glycolysis and carbon, tyrosine or glutathione metabolisms (dark blue bar), suggesting a general
216   collapse of essential cell functions. Overall, CG display a biphasic transcriptional response
217   along tumour progression, marked by initial enrichment of specific genes followed by later
218   collapse of core cellular functions.

219   In light of our results on CG apoptosis, we first decided to check the expression profiles of
220   members of the apoptotic pathway (**Fig. 5D and S3B**). Analysis across these conditions
221   revealed that several key apoptotic components were upregulated in tumour compared to non-
222   tumour tissues, with different temporal dynamics (at day 1 and/or day 6), fitting our earlier data.
223   This includes core cell death activators *reaper*, *grim* and *sickle* (*skl*), the initiator caspases
224   *dronc*, *dredd* and *strica*, the effector caspase *dcp-1* as well as the pro-apoptotic Bcl2
225   orthologues, *buffy* and *debcl* (**Fig. 5D**, green boxes). Very few anti-apoptotic factors were
226   upregulated in tumour conditions, such as *bruce* (**Fig. 5D**, dark blue box).

The JNK pathway is physiologically active in cortex glia and is downregulated during tumour progression

229   Remarkably, we noticed that several core members of the c-Jun N-terminal kinase (JNK)
230   pathway showed altered expression in tumour conditions (**Fig. 5D**, magenta boxes). This highly

13

conserved MAPK (mitogen-activated protein kinase) pathway is a prominent intracellular player in the response to a range of stress signals and in the regulation of several key cellular processes, including cell proliferation, differentiation, survival, and death. The specific outcomes of JNK activation depend on the stimulus, cell type, and the particular kinases involved. Notably, JNK regulates core pathways playing a crucial role in both cell proliferation and cell death (*89, 90*), and as such has been since long highly involved in tumourigenesis, in multiple and sometimes conflicting ways (*91–94*). In particular, its known prominent role in cell competition made it a very promising candidate in light of our previous results.

Typically, the activation of MAPK signalling pathways begins when a receptor is activated by a variety of extracellular stimuli (*95*). This triggers the recruitment of adaptor proteins and the activation of small GTP-binding proteins called G-proteins. This induces a cascade of protein, which can consist of up to four successive levels of kinases. For the JNK pathway, JNKKKs (MEKKs, MLKs, DLK, TAK1, ASK1) phosphorylate and activate the JNKKs, which in turn phosphorylate and activate JNKs. Activated JNKs subsequently phosphorylate a diverse array of substrates, including transcription factors (*e.g.,* c-Jun, p53, c-Myc), Bcl-2 family proteins and other kinases and signaling proteins. Analysis of the expression profiles of components of the *Drosophila* JNK pathway showed that the upstream JNKKK dTak1 was upregulated at day 6, whereas JNK itself (*basket, bsk*) was downregulated at day 3 and day 6. Additionally, its negative regulator and transcriptional target *puckered* (*puc*) was downregulated at day 6 during tumour progression (**Fig. 5D**, magenta boxes; **Fig. 5E** and **Fig. S3B**).

puc encodes a JNK phosphatase which negatively regulates the activity of the JNK pathway and is itself a transcriptional target of JNK, creating a negative feedback loop (*96, 97*). As such, *puc* expression has been used as a readout of JNK activation. To assess JNK activity, we relied on the commonly used lacZ enhancer trap line *puc^E69* (*puc-LacZ*), in which the expression of the β-galactosidase is under the control of *puc* enhancer sequences. This line is also an insertional, homozygous lethal mutant for *puc* (*98*) and therefore, *puc-LacZ* was used in heterozygous. We determined β-Galactosidase (β-Gal) levels in non-tumour (control) and tumour conditions at day 6 of adulthood (**Fig. 5F**), the timepoint when *puc* downregulation is observed in the TaDa-Pol II data (**Fig. 5D**, magenta boxes). Co-staining with Repo to assess β-gal expression in glia revealed that *puc-lacZ* was active in most, though not all, glia cells in control condition. However, in tumour condition, both the proportion of β-Gal$^+$ glia and the overall *β-gal* expression levels were sharply reduced (**Fig. 5G-H**). In addition, co-staining with ElaV showed that *β-gal* was expressed in most neurons under control conditions, with higher

14

264   expression levels than in glia (**Fig. 5I-J**). To our surprise, the proportion of β-gal^+ neurons

265   significantly decreased in tumour conditions, accompanied by a reduction in expression level,

266   although less pronounced than in the glia. Of note, no β-gal signal was detected in CSPCs

267   suggesting that JNK is not activated in tumour cells (**Fig. 5F**).

268   Taken together, these data suggest that the JNK pathway is normally active in both glia and

269   neurons, but becomes downregulated in both cell types during tumour growth, with a more

270   pronounced decrease in glia.

271   **Inhibition of the JNK pathway in CG elicits a dual, temporally dynamic effect on tumour**

272   **progression and reveals its contribution to host tissue resistance and integrity**

273   JNK pathway activation has been traditionally linked to promoting the elimination of less fit

274   "loser" cells by more competitive "winner" cells in the context of cell competition (*99, 100*).

275   We thus wondered whether JNK signalling balances resistance and cell competition and how

276   the observed progressive downregulation of JNK in the CG impacts tumour progression. To

277   address this question, we adopted a strategy similar to *reaper* overexpression, blocking JNK

278   activation from the onset of adulthood across the entire CG population. We used the QF system

279   to express a dominant-negative form of Bsk in the CG (*cyp > bsk^{DN}*), while simultaneously

280   inducing tumour formation through the GAL4/UAS system (*poxn > pros^{RNAi}, pros^{poxn}* tumours)

281   (**Fig. 6A**). As before, *bsk^{DN}* expression was induced by heatshock from adult eclosion (day 0).

282   The analysis at day 6 of tumour volume (Dpn$^+$ cells) when *bsk^{DN}* was expressed in the CG (*poxn*

283   *> pros^{RNAi}, cyp > bsk^{DN}*) revealed a mild yet significant increase compared to a control tumour

284   condition (*poxn > pros^{RNAi}, pros^{poxn}* tumours) (**Fig. 6B**). This was accompanied by a significant

285   decrease in both glial volume (**Fig. 6C**) and nuclei number (**Fig. S4A**). Glial individual nuclear

286   volume was actually increased (**Fig. S4B**), reflecting a shift in the glial population, with CG

287   being depleted and other subtypes possessing large polyploid nuclei, such as subperineurial

288   glia, becoming relatively enriched. No significant changes were detected in neuronal volume

289   (**Fig. 6D**) or cell apoptosis (number of Dcp-1+ cells, **Fig. 6E**), despite a slight trend towards

290   decreased neuronal volume. These results indicate that active JNK signalling in CG does not

291   induce apoptosis nor cell elimination, but instead plays an anti-tumour role, constraining its

292   growth.

293   Based on these findings, we next evaluated the impact of JNK function at a later time point,

294   day 9 of adulthood, anticipating a stronger effect on the various cell populations. Suprisingly,

295   we found a clear, significant decrease in tumour volume when *bsk^{DN}* was expressed in the CG,

15

296 opposite to the increase observed at day 6 (**Fig. 6B**). We calculated that the mean growth rate

297 of control tumour between day 6 and day 9 was close to 2, while tumours expressing bsk^{DN} in

298 the CG had a reduced mean growth rate of 1.2 (see **Table S2**). These data indicate that JNK

299 signalling in CG becomes beneficial to tumour growth at later stages, and that its sustained

300 downregulation ultimately hinders tumour growth. This pro-tumour role was not accompanied

301 by any change in glial volume or apoptotic cell counts compared to control tumours (**Fig. 6C,**

302 **E**), suggesting that it is independent of CG elmination. However, we recorded a significant

303 decrease in neuronal volume at day 9 when bsk^{DN} was expressed in the CG (**Fig. 6D**).

304 Importantly, neuronal volume was not decreased in control tumours compared to non-tumour

305 conditions at day 9, showing that at this stage neurons remain protected from tumour-induced

306 loss when JNK is active (**Fig. S4C-D**). Thus JNK signalling in CG provides a non-cell

307 autonomous protection to neurons during tumour progression.

308 We then wondered whether this neuroprotective role was specific to tumour conditions, or also

309 present under physiological, non tumour conditions. We induced bsk^{DN} in CG from day 0 of

310 adulthood using the TARGET system, in which the onset of GAL4 activity is controlled through

311 temperature shift by a thermosensitive version of its inhibitor GAL80 (*101*) (**Fig. S5A**). We

312 measured the volume, nuclei number and average nuclear volume of glial cells (Repo⁺) per

313 VNC, finding no significant differences between control and bsk^{DN}except at day 9 (at 29°C),

314 when bsk^{DN} expression led to more glial nuclei of smaller volume (**Fig. S5B-D**). Neuronal

315 volume also remained largely unchanged between control and bsk^{DN}, although a slight, non-

316 significant decrease was observed at day 9 (**Fig. S5E**). However, expressing bsk^{DN} in the CG

317 resulted in higher numbers of apoptotic Dcp-1⁺ cells in the VNC at all time points examined

318 (**Fig. S5F**). These results suggest that physiological JNK signalling may exert a mild

319 neuroprotective effect by limiting apoptosis, consistent with our observations under tumour

320 conditions.

321 Together, these data reveal that during adulthood, JNK signalling is active in glial cells where

322 it has a neuroprotective function and provides partial resistance to tumour growth. However,

323 during tumourigenesis, JNK signalling is silenced in glia surrounding the tumour, leading to

324 increased tumour growth and consequently reduced glial numbers. While JNK silencing in CG

325 during tumourigenesis initially facilitates tumour growth, in the long term it contributes to a

326 global collapse of the nervous system along with restricting tumour progression.

1 **DISCUSSION**

2 Using a *Drosophila* CSC-driven tumour model, this study explores how host cells within the

3 TME influence tumour progression. We first found that the cortex glia (CG), a major glial

4 subtype in direct contact with the tumour, remodel their membranes and infiltrate the tumour

5 mass during tumour growth. However, this infiltration declines over time, concurrent with CG

6 cells undergoing apoptosis and subsequent elimination. Strikingly, CG cell death plays a pivotal

7 role in tumour progression, as accelerating or preventing it, increases or decreases tumour

8 growth respectively. This finding reveals that CG cells possess an intrinsic capacity for

9 resistance, which tumour cells ultimately overcome via CSC-driven cell competition, allowing

10 tumour expansion. These two tumour-host interaction phases are reflected by the CG

11 transcriptome over time. Initially, a specific CG signature is present, but it later shifts to a

12 general downregulation of core cellular functions and metabolic pathways, including the JNK

13 pathway. We found that the role of JNK downregulation in tumour progression is also two-

14 faced. Initially, active JNK signalling confers resistance to tumour growth, and its

15 downregulation is thus beneficial to the tumour. However sustained downregulation ultimately

16 appears detrimental to the tumour, restricting its growth. Importantly, his latter phase is

17 accompanied by neuronal loss, revealing a neuroprotective role of JNK signalling in the CG.

18 Thus, our study highlights interlinked biphasic behaviours at both host tissue and tumour levels,

19 which shape tumour growth dynamics. The host tissue possesses resistance mechanisms which

20 are eventually overcome by sustained CSC-driven competition, ultimately leading to collapse

21 of host tissue and its supportive functions, and curbing tumour growth itself (**Fig. 7A-C**).

22 **Growth of tumour clones**

23 The tumour, observed in the adult stage as a whole, is actually the result and sum of the growth

24 of six individual tumours from larval stage. Using a multicolour clonal analysis, we found that

25 these tumours do not seem to intermingle but remain well-delineated, with CG membrane

26 separating them, at least during the time of our analysis (**Fig. 1J-K** and **Fig. S1B-D**). In larval

27 stage, normal NSC lineages rely on differential adhesion to prevent merging with neighbouring

28 lineages, independent of CG wrapping, and individual *pros* tumours similarly remain separated

29 (*78*). In our model, it would be interesting to see whether this clonal organisation is indeed

30 intrinsic and controlled by adhesion complexes, or relies on the maintenance of the CG barrier

31 between clones. Future studies on the adhesive molecular signature of these tumours are needed

32 to better understand the inter-clonal organisation, and could provide insight into why and how

33 CG membranes can infiltrate the tumour at this stage.

Cancer stem cell-driven cell competition

34

35 Previous studies on epithelial tumours in the *Drosophila* gut and in mouse intestinal organoids

36 have shown that tumour mutant clones kill their healthy counterparts, a cell competition-based

37 phenomenon essential for tumour growth (*42*, *44*). Here, we find that *pros^{poxn}* tumours

38 progressively induce apoptosis and elimination of CG cells, and that, in turn, glial death

39 promotes tumour growth. Cell competition-induced death within the TME therefore could be a

40 fundamental process driving tumour growth across various cancers –including CNS tumours,

41 where this mechanism had not been previously identified and where host cells are non-epithelial

42 and of different origin.

43 Yet, molecular mechanisms appear to differ. In gut epithelial tumours, the JNK pathway is

44 active both in tumour cells and surrounding cells, where it is required for their growth and their

45 elimination, respectively (*42*). Several other epithelial contexts of cell competition, with

46 genetically-induced mosaic populations of either less fit/loser (*eg*, *minute* (*40*), *scrib* mutants

47 (*102*, *103*)) or super-competitor/winner (*eg*, *myc* (*104*, *105*)) cells *versus* wild-type cells (thus

48 respectively behaving as winner or loser), have shown that JNK pathway activation in loser

49 cells is key for their engagement into apoptotic processes and elimination (reviewed in (*39*, *99*,

50 *100*, *106*, *107*)). When wild-type cells act as winners, JNK is also active in these cells,

51 mediating the engulfment of loser cells. Finally, models of compensatory proliferation

52 following apoptosis (also known as apoptosis-induced proliferation) have involved JNK

53 pathway activation in the apoptotic and/or responsive cells, this time downstream of apoptosis

54 (*100*, *106*, *108*).

55 In the CNS, JNK is not active in tumour cells (**Fig. 5F**). Moreover, JNK signalling is

56 constitutively on in CG cells, rather becomes downregulated during tumour progression (**Fig.**

57 **5**), and does not contribute to CG elimination, as its inhibition fails to rescue glial loss (**Fig.**

58 **6C**). This highlights a role of JNK beyond its established functions in cell competition. How

59 tumour cells induce apoptosis in CG cells remain to be elucidated. Potential mechanisms

60 include direct cell-cell interactions through transmembrane partners, paracrine short-range

61 diffusive signals and mechanical stress. Our finding that the concentration in CSCs, rather than

62 overall tumour volume *per se*, correlates with the level of glial loss (**Fig. 3F-G**) is striking and

63 suggest that CSCs are essential and likely a key source of (possibly paracrine) apoptotic signals.

Glial cells and JNK signalling spearhead host tissue resistance to tumour growth

64

65 Although competition from the tumour ultimately eliminates and overpowers CG cells, these

66 cells exhibit a certain potential to hinder tumour progression. This resistance to tumour growth

67   (and not to death) is demonstrated by the effects of either removing or preserving CG cells in

68   the TME (**Fig. 4A-F**). This exciting finding suggests that targeting the host tissue, and, perhaps

69   counterintuitively, blocking cell death, could represent an interesting angle for therapeutic

70   approaches. A prerequisite would be to identify the mechanisms behind such resistance, which

71   may be multifactorial and not mutually exclusive, including mechanical- and signalling-driven

72   processes. One intrinsic, already present mechanism seems to involve the JNK pathway. JNK

73   signalling is normally active and present in CG, where it where it exerts an anti-tumour effect,

74   at least during the initial stages (**Fig. 6A-B**). This anti-tumour role does not seem to involve

75   apoptosis (**Fig. 6E**), and other known functions of JNK signalling, such as regulation of

76   proliferation and cytoskeleton organisation, require further investigation. Beyond already pre-

77   existing resistance mechanisms, CG could actively set up additional defense or attack systems

78   in response to tumour growth. The existence of a distinct transcriptomic signature early during

79   tumour progression (day 1) (**Fig. 5B-C**) may provide insight into these mechanisms. This

80   signature is characterized by the upregulation of immunity-related genes, including

81   antimicrobial peptides, and genes involved in lipid metabolism. It has been shown that the

82   *Drosophila* immune system reacts to and kill epithelial tumour cells with the release of

83   antimicrobial peptides (*109*), suggesting that their upregulation in the CG could contribute to

84   targeting the tumour. Moreover, activation of conserved immune pathways across diverse

85   competition models has been identified as a driver of loser cells apoptosis (*110*). However the

86   functional relevance of this genetic signature for CG resistance will have to be disentangled

87   from other opposite roles of the CG in tumour support. This is a general interrogation both for

88   pre-existing or set up cellular and molecular processes, as we uncovered with the biphasic role

89   of the JNK pathway.

90   **Late JNK signalling: turning pro-tumour or avoiding whole system's collapse?**

91   Unexpectedly, we found that JNK downregulation led to a dramatic slowdown, nearly to a halt,

92   of tumour growth at a later phase (**Fig. 6A-B** and **Table S2**), showing JNK switches to a pro-

93   tumour role. Theis finding highlights the dual role of the TME in regulating tumour progression.

94   JNK in the CG could help tumour growth in many ways, by trophic support, architectural

95   remodeling, or signaling mechanisms. Notably, we observed an infiltration of the tumour clones

96   by CG membranes, something we do not see for non-transformed lineages or very small

97   tumours (**Fig. 1D, H, K** and (*78*)). CSCs may acquire some properties (signals and/or loss of

98   inter-adhesions) which attract or/and are permissive for CG to infiltrate; in turn such infiltration

99   could sustain tumour growth by locally providing important factors. Interestingly, in a glioma

19

100   model (*111*) where CG cells themselves undergo transformation, JNK activation promotes CG

101   membrane remodeling and the formation of an infiltrating interconnected network which

102   support tumour growth while causing neurodegeneration (*112*). It would be interesting to test

103   whether JNK signalling regulates CG membrane network in our model.

104   Why the loss of JNK signalling is ultimately detrimental to tumour growth, as such a late stage,

105   is left to be investigated. An intriguing observation is that such effect is concomitant to the loss

106   of neurons, whose survival appears to depend on JNK signalling in the CG (**Fig. 6A, D**). Of

107   note, JNK signalling in glia promotes neuronal phagocytosis and clearance during *Drosophila*

108   development (*113, 114*), highlighting complex neuron-glia dynamics. In adult, JNK

109   neuroprotective role also takes place in normal, non-tumour condition, although to a lesser

110   extent (**Fig. S5E, F**). A compelling hypothesis is that neuronal loss is causative of tumour

111   slowdown, rather than JNK directly promoting tumour progression. Recent studies have indeed

112   connected the presence and activity of neurons to the promotion of tumour growth,

113   emphasizing the cooption of normal neuron-glia interaction in these processes (reviewed in (*27,*

114   *28*)). Our model could fit in this picture, with tumour growth dependent on neurons.

115   Notably, neurons in control tumours do not seem to die until day 9, suggesting that they are

116   either shielded from tumour growth longer than glial cells or that neuronal loss is too minimal

117   to detect. Yet, the slight trend towards neuronal volume decrease for $Syp^{RNAi}pros^{poxn}$ tumours

118   (**Fig. S2E**), where tumours grow and glial cells die much faster, may suggest that neurons could

119   eventually be lost as well. It would be interesting to check neuronal volume and apoptosis

120   beyond day 9 in $pros^{poxn}$ tumours to determine whether neuronal loss eventually occurs and

121   coincides with host death. In $pros^{poxn}$ tumours, the death of CG cells reduces JNK signalling at

122   the tissue level, and surviving glial cells exhibit lower JNK activity, as indicated by reduced

123   *puc* expression in TaDa-Pol II profiling and reporter assays (**Fig. 5D, F-H**) –what would

124   dramatically decrease JNK signalling on the long run and affect neurons.Thus, the level of JNK

125   signalling may be a key mechanism deciding on neuronal fate under tumour condition, rather

126   than sheer tumour growth alone. Curiously, JNK levels are also lowered in neurons, albeit less

127   than in glial cells (**Fig. 5F, I-J**). It remains unclear whether JNK downregulation in one cell

128   type influences the other, or what ultimately triggers cell death. Nevertheless, the role of JNK

129   signalling in CG for neuronal survival is clear (**Fig. 6D**), independently of potential relays.

130   Ultimately, neuronal fate may determine the overall trajectory of tumour progression

131   By analysing cell types, cellular processes, gene expression profiles and pathway functions, our

132   study converges on the critical importance of timing in tumour growth, specifically highlighting

20

133   multiple biphasic behaviours. Within the tumour microenvironment, glial cells transition from

134   an initial resistance and active response phase to eventual collapse, while the JNK pathway

135   exerts a dual, progressive influence on both tumour and neurons. The complex, dynamic and

136   sometimes antagonstic functions of the different cellular and molecular players in the TME

137   interact and compete with the CSC-driven tumour. The timing of these evolving interactions

138   will shape tumour growth and outcome. This central concept, together with the presence of

139   intrinsic resistance mechanisms in the host tissue, highlights the importance of early

140   intervention in tumour development. Enhancing host tissue defense mechanisms emerges as a

141   therapeutic alternative to directly targeting the tumour.

1 **METHODS**

2 **Fly lines and husbandry**

3 *Drosophila melanogaster* lines were kept and raised in vials containing standard cornmeal food

4 medium. Two copies of each stock were maintained at 18°C and flipped into fresh food vials

5 every 4-6 weeks until their use in crosses and experimental procedures. Working stocks were

6 kept at 25°C.

7 Parental lines were crossed in vials and allowed to lay eggs for 2 days at 25°C, then flipped in

8 another vial. Larvae and pupae from each egg laying were left to develop in these vials at 25°C,

9 unless specified in Table S1. Day 0 of adulthood was defined as at the day of eclosion from the

10 pupal case for each adult.

11 18°C was used to keep the thermosensitive allele of GAL80 (GAL80^{ts}), a repressor of GAL4,

12 active (to switch off GAL4 expression), while 29°C was used for its inactivation (to switch on

13 GAL4 expression). Temperature switch was performed at eclosion (day 0).

14 For induction of QUAS-reaper, QUAS-p35, QUAS-bskDN and QUAS-puc, adult virgin

15 females at eclosion (day 0), were heat shocked for 4h at 37 °C and aged to the desired day

16 before dissection.

17 Detailed genotypes, crosses and culture regimens are listed in Table S1. All the experiments

18 were performed only on female flies.

19

20 The lines used in this study are listed below:

Strains	Source	Stock number/Reference
w^{1118}	BDSC	5905
yw, hs-FLP	Andrea Brand lab	
Nervana2::GFP (Nrv2::GFP)	BDSC	6828
puc^{E69} (puc-lacZ)	Stéphane Noselli lab	(*98*)
cyp4g15(cyp)-myr::tdTomato	Spéder lab	(*70*)
tubulin-GAL80$^{thermosensitive(ts)}$	BDSC	65406
cyp4g15(cyp)-GAL4	BDSC	39103
poxn-GAL4	BDSC	66685
actin-LexA	BDSC	62567
cyp4g15(cyp)-QF2	Pauline Spéder lab	(*70*)
cyp4g15-FRT-STOP-FRT-QF2	Pauline Spéder lab	This study
UAS-dicer	BDSC	24650
UAS-bsk^{DN}	BDSC	6409
UAS-prospero RNAi	VDRC	101477
UAS-Syncrip-RNAi	VDRC	33011

UAS-raeppli-NLS 53D	BDSC	55087
LexAOp-GC3Ai	Romain Levayer lab	(85, 115)
QUAS-His2Av::mCherry	BDSC	93911
QUAS-Dam	Pauline Spéder lab	This study
QUAS-Dam-PolII	Pauline Spéder lab	This study
QUAS-bsk^{DN}	Hermann Steller lab	
QUAS-p35	Hermann Steller lab	(116)
QUAS-reaper	Hermann Steller lab	(116)

21

DNA cloning and *Drosophila* transgenics

22

23 *cyp4g15-FRT-STOP-FRT-QF2* was generated in the same fashion as *cyp4g15-FRT-STOP-*
24 *FRT-LexA* (*70*). Part of the cyp4g15 enhancer (GMR55B12, Flybase ID FBsf0000165617) was
25 amplified from genomic DNA extracted from cyp4g15-GAL4 adult flies, with a minimal
26 Drosophila synthetic core promoter [DSCP93] fused in C-terminal. A FRT STOP cassette was
27 amplified from an *UAS-FRT.STOP-Bxb1* plasmid (gift from MK. Mazouni) and the QF
28 sequence was amplified from the entry vector pENTR L5-QF2-L2 (gift from S.
29 Stowers / M. Landgraf; Addgene 32305). The two amplicons were joined by overlapping
30 PCRs. This *FRT-STOP-FRT-QF2* amplicon was inserted together with the *cyp4g15^{DSCP}*
31 enhancer in the destination vector pDESThaw sv40 (gift from S. Stowers) using the Multisite
32 gateway system (*117*) to generate a *cyp4g15^{DSCP}-FRT-STOP-FRT-QF2* construct. The
33 construct was integrated into the fly genome at either an attP2 or attP40 docking site through
34 PhiC31 integrase-mediated transgenesis (BestGene). Several independent transgenic lines were
35 generated and tested, and one was kept.
36 QUAS-Dam and QUAS-Dam::PolII were created by amplifying the Dam and Dam::PolII
37 sequences respectively from the pUASt-attB-LT3-Dam and pUASt-attB-LT3-Dam::PolII
38 plasmid (*87*). Each amplicon was inserted into the entry vector pDONR P5-L2 to create entry
39 vectors pENTR-L5-Dam-L2 and pENTR-L5-Dam::PolII-L2. Each of these pENTR was
40 combined with the entry vector pENTR-L1-10XQUAS-R5 and the destination vector
41 pDESThaw sv40 (both gifts from S. Stowers) using the Multisite gateway system (*117*) to
42 generate the QUAS-Dam and QUAS-Dam::PolII constructs. The constructs were integrated
43 into the fly genome at either an attP40 docking site through PhiC31 integrase-mediated
44 transgenesis (BestGene). Several independent transgenic lines were generated and tested, and
45 one was kept.

Transcriptional profiling

We used Targeted DamID (*87*, *88*, *118*) to profile transcription in cortex glia at different timepoints, during tumour progression. *QUAS-Dam* and Q*UAS-Dam ::Pol II* flies were crossed to *tubulin-GAL80^{ts}*; *cyp4g15-GAL4* flies. Induction was performed through a 4 h heat shock at 37°C at day 1 and day 6 of adulthood. The flies were dissected after 14 h of induction and the VNCs were stored at -80°C in 50ul of PBS, until samples were ready to be prepared for the DNA extraction. Processing of genomic DNA were performed as previously described (*88*). Two biological replicates were performed for each timepoint. For each condition, DamID-seq samples were processed via the damid_seq pipeline v1.5.3 (*118*), that automatically handles sequence alignment, read extension, binned counts, normalization, pseudocount addition and background reduction (Pol-II / Dam only). Average Pol-II occupancy and FDR were calculated for each gene of Drosophilia melanogaster genome (DmR6 release) with the polii.gene.call script (*88*, *119*). Differentially expressed genes were identified via the NOIseq R package (*120*): RNA pol II gene occupancy scores were scaled, and inverse log values used as input to NOIseq with parameters of upper quantile normalization and biological replicates. DEGs were called with a q-value of 0.90. The functional enrichment of up and down regulated genes was calculated with the DAVID analysis tool (*121*) using Gene Ontology, KEGG and Reactome functional gene sets and Drosophila melanogaster annotations as background. Annotation categories were considered as enriched when at least 2 genes were involved in and passing the EASE score threshold of 0.1. Treemap plots and heatmaps were generated using R (v4.1.3) (*122*) and the treemap (v2.4-3) (*123*) and pheatmap (v1.0.12) (*124*) packages. KEGG maps have been designed with Pathview R package (*125*).

Fixed tissue immunostaining

Adult CNSs were fixed for 30 minutes in 4% methanol-free formaldehyde (ThermoFisher 28908) while rocking at room temperature. They were washed in PBS once and permeabilized in PBS containing 1% Triton (Sigma T9284) three times for 10 minutes each. CNSs were incubated with blocking solution (PBS-Triton 1%, 5% Bovine Serum Albumin (Sigma A3608), 2% Normal Goat Serum (Abcam ab7481) for 1 hour at room temperature while rocking. Primary antibody dilution was prepared in blocking solution and CNSs were incubated at 4°C for 48 hours, then washed three times with PBS-Triton 1% while rocking. Secondary antibodies were diluted in blocking solution and CNSs were incubated at room temperature for 2 to 3 h. CNSs were washed three times with PBS while rocking and kept in PBS at 4°C until mounted.

78 Homemade mowiol mounting medium (Sigma 81381) was used to mount the CNSs between

79 borosilicate glass slides (number 1.5; VWR International) and coverslips.

80 Primary antibodies used were: guinea pig anti-Dpn (1:1000,(*70*)), rat anti-ElaV (1:100,

81 7E8A10-c, DSHB), mouse anti-Repo (1:100 (DSHB, 8D12-c), rabbit anti-Dcp-1 (1:100, Cell

82 Signaling 9578), rabbit anti-β-galactosidase (1:200, ThermoFisher Scientific A-11132).

83 Fluorescently-conjugated secondary antibodies Alexa Fluor 405, Alexa Fluor 488, Alexa Fluor

84 546 and Alexa Fluor 633 (ThermoFisher Scientific) were used at a 1:200 dilution. DAPI (4′,6-

85 diamidino-2-phenylindole, ThermoFisher Scientific 62247) was used to counterstain the nuclei.

86 **Image acquisition and processing**

87 Confocal images were acquired using a laser scanning confocal microscope (Zeiss LSM 880,

88 Zen software (2012 S4)) with a Plan-Apochromat 40x/1.3 Oil objective. All VNCs were imaged

89 as z-stacks with an optimal distance between each slice of 1 μm and using tiles, with 5-10 %

90 overlap. Images were analysed and processed using Fiji (Schindelin, J. 2012), Volocity (6.3

91 Quorum technologies), and Imaris (version 10.2.0). Denoising was used for some images using

92 the Remove noise function (Fine filter) in Volocity. Images were assembled using Adobe

93 Illustrator 29.6.1.

94 **Quantification of tumour, glial and neuronal volumes**

95 Dpn, Repo, ElaV and His::mCherry (under the control of *cy4g15* enhancer sequences, *cyp >*

96 *His::mCherry*) signals were used to measure nuclear volumes for tumour, glia, neurons and CG

97 cells respectively. For Repo and His::mCherry signals, in which the nuclei are better separated

98 in space, the nuclear volume for individual cell was also calculated.

99 Two different protocols were used.

100 For Fig. 1C, 2B-C, S2, 3F-G and 4, nuclei volume quantification was achieved with a Python

101 script deposited on Zenodo (10.5281/zenodo.16733817) together with its operating manual.

102 For Fig. 6, S4 and S5, raw confocal Zeiss files (.czi) were opened in Imaris (version 10.2.0).

103 Once converted to an Imaris *.ims file, nuclei segmentation was performed by applying the

104 Surface Wizard tool to the desired cell channels. The following settings were used for all the

105 images: 0.415 μm for smooth surface details; background subtraction and the diameter of

106 largest sphere was 1.56 μm; enabled split touching object and morphological split; seed points

107 diameter 2.08 μm. The processed images were visually examined alongside the original

108 channels to ensure correct identification of cell types. Statistics for individual images were

109 exported in either Microsoft Excel or CSV format. The data were then imported into GraphPad

110 Prism for quantitative/statistical analysis.

Quantification of Puc-lacZ signal

Image analysis to assess puc expression level in glia and neurons was performed on Fiji to quantify volumetric and fluorescence intensity data from 3D image stacks, following four steps.

1. Image Selection and Preprocessing. Individual channels (Puc-lacZ and either Repo or ElaV) were duplicated two times. Thresholding was determined manually and applied to each channel, resulting in image pairs of the original channel image and the threshold binary mask for *puc* expression and the cell population of interest (for exemple: Puc threshold Mask 1 and its corresponding fluorescence image with Elav threshold Mask 2 and its corresponding fluorescence image). These masks are used to define regions of interest (ROIs) for subsequent analysis.

2. Mask Combination and Volume Calculation. An intersection of the two selected masks was generated using the "AND create stack" operation in Fiji (Image Calculator tool), resulting in a combined mask ("Puc and Repo or ElaV Mask"). The individual and combined volumes of Puc-lacZ Mask, Repo or ElaV Mask, and the intersection were estimated by iterating through each z-slice of the stacks and summing the integrated density values normalized by 255 (assuming 8-bit images for the binary masks).

3. Mask Inversion and Fluorescence Image Processing. All mask images were inverted across the stack to ensure correct masking behaviour during fluorescence processing. Fluorescence signals were isolated within each mask by performing a "Transparent-zero create stack" operation followed by subtraction of the original mask from the resulting stack. This was done for each mask-fluorescence image pair and for the intersection mask with both fluorescence images.

4. Intensity and Mean Fluorescence Quantification (This was not collected for the puc measurement). For each masked fluorescence image, the macro iterated through all z-slices to calculate the sum of normalized integrated density (IntDen/Area) (also from the Image Calculator tool) and mean gray value (Mean) for each slice. These values were accumulated across the stack to compute the total intensity and average mean intensity per ROI.

The following measurements were reported:

- Total and mean fluorescence intensity for Puc-lacZ Mask

- Total and mean fluorescence intensity for Repo or ElaV Mask

- Total and mean fluorescence intensity of Puc-lacZ in regions positive for both masks (Puc-lacZ Mask ∩ ElaV or Repo Mask).

% of Puc-LacZ glia or neurons ware calculated by dividing the total volume of "Puc and Repo or ElaV Mask" by the total volume of Repo or ElaV Mask.

26

145   Mean Puc-LacZ intensity in glia or neurons was directly obtained from mean fluorescence

146   intensity of Puc-lacZ in regions positive for both masks (Puc-lacZ Mask ∩ ElaV or Repo Mask).

Quantification of apoptotic cells

148   Cells marked by Dcp-1 or GC3Ai were manually counted throughout the z-stack. The distance

149   between apoptotic tumour cells was measured by counting the smallest number of nuclei in-

150   between.

Statistical tests and experimental reproducibility

152   Statistical tests used for each experiment are stated in the figure legends. All statistical tests

153   were performed using GraphPad Prism 10.3.1 except for linear correlation (Fig. 3F-G). No

154   samples were excluded except when mentioned in the methods or figure legends (removal of

155   outliers). No sample-size calculations were performed *a priori*. Sample sizes were determined

156   by the number of processed samples (around 5-8 staged adult VNCs per experiment following

157   previous standards (*61–63*)).

158   For comparing two conditions, an unpaired Student t-test was used when they passed the

159   normality test (D'Agostino and Pearson test) and Mann-Whitney U test when they did not pass

160   the normality test. For comparing more than two conditions, a one-way ANOVA with Tukey's

161   multiple comparisons test was used on normal data and a Kruskal–Wallis H test with Dunn's

162   multiple comparisons test for data which did not pass normality.

163   The correlations between the glia and tumour volumes were tested using a linear model: the

164   glia volume was used as the dependent variable and both condition and tumour volume as

165   explanatory variables, as well as their interaction.

166   n/N numbers are indicated on the figure and their correspondence in the figure legends.

Data representation

168   All images displayed are representative.

169   Box plots show minimal value (bottom whisker), first quartile (25th percentile, lower limit of

170   the box), a median of the interquartile range (middle horizontal line), third quartile (75th

171   percentile, the upper limit of the box) and maximal value (top whisker). Individual values are

172   superimposed.

173   For dot plots, the identity of the dots is described in the legends of the figure and the horizontal

174   line corresponds to the median.

175   Significant and noteworthy p-values are displayed directly on the graph.

27

Acknowledgments

Author Contributions

Conceptualization: MG, PS

Methodology: MG, CM, PS. CM provided expertise on the tumour model.

Investigation: MG, SJ, MH. MG performed experiments of Figures 1; S1; 2A-C; S2; 3; S3; 4; S4; 5A-D and 6. SJ performed experiments of Figures 1I; 2D-F; S4; 5F-J; S5 and 6. MH helped with experiments of Figures 1I; 2D-F; S4; 5F-J; S5 and 6.

Formal Analysis: DM performed the analysis of the TaDa-PolII datasets.

Visualization: MG, SJ, PS

Funding acquisition: PS

28

207   Project administration: PS

208   Supervision: PS

209   Writing – original draft: MG, PS

210   Writing – review & editing: MG, CM, PS

211   **Declaration of Interests**

212   The authors declare no competing interest.

213   **Data and materials availability**

214   The TaDa-PolII dataset is available as Datasets S1 and S2. The scripts for volume quantification

215   will be accessible on Zenodo (10.5281/zenodo.16733817). Quantifications are available in the

216   Data source spreadsheet. *Drosophila* transgenic lines made for this study are available upon

217   request to the corresponding author and will be deposited in BDSC. The image datasets

218   generated during and/or analysed during the current study are available from the corresponding

219   author on reasonable request.

220   **Supplemental information**

221   Supplemental Figures S1–S5 and legends

222   **Dataset S1. Excel file containing the differential expression analysis for the TaDa**

223   **experiments.** The columns contain the different outpit avlues from NOISseq analysis.

224   **Dataset S2. Excel file containing the Gene enrichment analysis for the TaDa experiments.**

225   Table S1. *Drosophila* genotypes, crosses and culture regimens per experiment

226   Table S2. Tumour growth rates

227   Data Source

228

REFERENCES

1.	M. J. van den Bent, M. Geurts, P. J. French, M. Smits, D. Capper, J. E. C. Bromberg, S. M. Chang, Primary brain tumours in adults. *The Lancet* **402**, 1564–1579 (2023).

2.	R. Ronsley, B. Cole, T. Ketterl, J. Wright, R. Ermoian, L. M. Hoffman, A. S. Margol, S. E. S. Leary, Pediatric Central Nervous System Embryonal Tumors: Presentation, Diagnosis, Therapeutic Strategies, and Survivorship—A Review. *Pediatr. Neurol.* **161**, 237–246 (2024).

3.	G. Jacques, O. Cormac, "Central nervous system tumors" in *Handbook of Clinical Neurology* (Elsevier B.V., 2013; https://pubmed.ncbi.nlm.nih.gov/23622303/)vol. 112, pp. 931–958.

4.	S. N. Gröbner, B. C. Worst, J. Weischenfeldt, I. Buchhalter, K. Kleinheinz, V. A. Rudneva, P. D. Johann, G. P. Balasubramanian, M. Segura-Wang, S. Brabetz, S. Bender, B. Hutter, D. Sturm, E. Pfaff, D. Hübschmann, G. Zipprich, M. Heinold, J. Eils, C. Lawerenz, S. Erkek, S. Lambo, S. Waszak, C. Blattmann, A. Borkhardt, M. Kuhlen, A. Eggert, S. Fulda, M. Gessler, J. Wegert, R. Kappler, D. Baumhoer, S. Burdach, R. Kirschner-Schwabe, U. Kontny, A. E. Kulozik, D. Lohmann, S. Hettmer, C. Eckert, S. Bielack, M. Nathrath, C. Niemeyer, G. H. Richter, J. Schulte, R. Siebert, F. Westermann, J. J. Molenaar, G. Vassal, H. Witt, M. Zapatka, B. Burkhardt, C. P. Kratz, O. Witt, C. M. V. Tilburg, C. M. Kramm, G. Fleischhack, U. Dirksen, S. Rutkowski, M. Frühwald, K. V. Hoff, S. Wolf, T. Klingebiel, E. Koscielniak, P. Landgraf, J. Koster, A. C. Resnick, J. Zhang, Y. Liu, X. Zhou, A. J. Waanders, D. A. Zwijnenburg, P. Raman, B. Brors, U. D. Weber, P. A. Northcott, K. W. Pajtler, M. Kool, R. M. Piro, J. O. Korbel, M. Schlesner, R. Eils, D. T. W. Jones, P. Lichter, L. Chavez, S. M. Pfister, The landscape of genomic alterations across childhood cancers. *Nature* **555**, 321–327 (2018).

5.	T. N. Ignatova, V. G. Kukekov, E. D. Laywell, O. N. Suslov, F. D. Vrionis, D. A. Steindler, Human cortical glial tumors contain neural stem-like cells expressing astroglial and neuronal markers in vitro. *Glia* **39**, 193–206 (2002).

6.	S. K. Singh, I. D. Clarke, M. Terasaki, V. E. Bonn, C. Hawkins, J. Squire, P. B. Dirks, Identification of a cancer stem cell in human brain tumors. *Cancer Res.* **63**, 5821–5828 (2003).

7.	H. D. Hemmati, I. Nakano, J. A. Lazareff, M. Masterman-Smith, D. H. Geschwind, M. Bronner-Fraser, H. I. Kornblum, Cancerous stem cells can arise from pediatric brain tumors. *Proc. Natl. Acad. Sci. U. S. A.* **100**, 15178–15183 (2003).

8.	S. K. Singh, C. Hawkins, I. D. Clarke, J. A. Squire, J. Bayani, T. Hide, R. M. Henkelman, M. D. Cusimano, P. B. Dirks, Identification of human brain tumour initiating cells. *Nature* **432**, 396–401 (2004).

9.	R. Galli, E. Binda, U. Orfanelli, B. Cipelletti, A. Gritti, S. De Vitis, R. Fiocco, C. Foroni, F. Dimeco, A. Vescovi, Isolation and characterization of tumorigenic, stem-like neural precursors from human glioblastoma. *Cancer Res.* **64**, 7011–7021 (2004).

10.	B. Manoranjan, C. Venugopal, N. McFarlane, B. W. Doble, S. E. Dunn, K. Scheinemann, S. K. Singh, Medulloblastoma stem cells: where development and cancer cross pathways. *Pediatr. Res.* **71**, 516–522 (2012).

11.	F. J. Swartling, M. Čančer, A. Frantz, H. Weishaupt, A. I. Persson, Deregulated proliferation and differentiation in brain tumors. *Cell Tissue Res.* **359**, 225–54 (2015).

270   12.   J. D. Lathia, S. C. Mack, E. E. Mulkearns-Hubert, C. L. L. Valentim, J. N. Rich, Cancer
271   stem cells in glioblastoma. *Genes Dev.* **29**, 1203–17 (2015).

272   13.   R. Azzarelli, B. D. Simons, A. Philpott, The developmental origin of brain tumours: a
273   cellular and molecular framework. *Dev. Camb. Engl.* **145**, dev162693 (2018).

274   14.   S. Mehta, C. Lo Cascio, Developmentally regulated signaling pathways in glioma
275   invasion. *Cell. Mol. Life Sci.* **75**, 385–402 (2018).

276   15.   J. Chen, Y. Li, T.-S. Yu, R. M. McKay, D. K. Burns, S. G. Kernie, L. F. Parada, A
277   restricted cell population propagates glioblastoma growth after chemotherapy. *Nature* **488**,
278   522–526 (2012).

279   16.   L. T. H. Phi, I. N. Sari, Y. G. Yang, S. H. Lee, N. Jun, K. S. Kim, Y. K. Lee, H. Y. Kwon,
280   Cancer Stem Cells (CSCs) in Drug Resistance and their Therapeutic Implications in Cancer
281   Treatment. *Stem Cells Int.* **2018** (2018).

282   17.   Q. R. Lu, L. Qian, X. Zhou, Convergence of Developmental Origins and Oncogenic
283   Pathways in Malignant Brain Tumors. *Wiley Interdiscip. Rev. Dev. Biol.* **8**, e342 (2019).

284   18.   K. E. de Visser, J. A. Joyce, The evolving tumor microenvironment: From cancer
285   initiation to metastatic outgrowth. *Cancer Cell* **41**, 374–403 (2023).

286   19.   S. Yuan, J. Almagro, E. Fuchs, Beyond genetics: driving cancer with the tumour
287   microenvironment behind the wheel. *Nat. Rev. Cancer* **24**, 274–286 (2024).

288   20.   J. D. Lathia, J. M. Heddleston, M. Venere, J. N. Rich, Deadly teamwork: neural cancer
289   stem cells and the tumor microenvironment. *Cell Stem Cell* **8**, 482–5 (2011).

290   21.   D. Hambardzumyan, G. Bergers, R. Stupp, E. Al., C. W. Brennan, E. Al., C. G. A. R.
291   Network, R. G. Verhaak, E. Al., M. Snuderl, E. Al., N. J. Szerlip, E. Al., A. Sottoriva, E. Al.,
292   A. P. Patel, E. Al., S. K. Singh, E. Al., J. D. Lathia, E. Al., C. Calabrese, E. Al., S. Bao, E. Al.,
293   H. F. Dvorak, R. Du, E. Al., G. Bergers, R. Wang, E. Al., Y. Soda, E. Al., L. Ricci-Vitiani, E.
294   Al., L. Cheng, E. Al., A. Kulla, E. Al., X. M. Liu, E. Al., F. J. Rodriguez, E. Al., N. J. Abbott,
295   G. Bergers, S. Song, X. Feng, E. Al., J. Liang, E. Al., G. Kohanbash, H. Okada, A. Mantovani,
296   E. Al., B. C. Kennedy, E. Al., F. Szulzewsky, E. Al., J. R. Engler, E. Al., N. A. Charles, E. Al.,
297   F. Ginhoux, E. Al., B. Ajami, E. Al., M. R. Elmore, E. Al., F. Geissmann, E. Al., S. Yona, E.
298   Al., N. Saederup, E. Al., R. Yamasaki, E. Al., M. Mizutani, E. Al., L. Yi, E. Al., X. Z. Ye, E.
299   Al., W. Zhou, E. Al., A. M. Mikheev, E. Al., D. J. Brat, E. Al., G. D. Yancopoulos, E. Al., F.
300   J. Wippold, E. Al., D. J. Brat, E. G. V. Meir, G. L. Semenza, S. Seidel, E. Al., A. Soeda, E. Al.,
301   E. E. Bar, E. Al., D. Zagzag, E. Al., E. E. Bar, G. L. Semenza, D. J. Brat, A. Filatova, E. Al., J.
302   M. Heddleston, E. Al., Z. Li, E. Al., B. Z. Qian, J. W. Pollard, A. Casazza, E. Al., B. Ruffell,
303   L. M. Coussens, L. B. Rivera, G. Bergers, V. A. Cuddapah, E. Al., M. Westphal, K. Lamszus,
304   S. S. Lakka, E. Al., R. Du, E. Al., M. Paez-Ribes, E. Al., J. L. Rubenstein, E. Al., C. Eckerich,
305   E. Al., S. D. Rose, M. K. Aghi, F. M. Iwamoto, E. Al., K. V. Lu, E. Al., M. Luo, E. Al., C.
306   Scheel, R. A. Weinberg, T. M. Mathiisen, E. Al., S. Watkins, E. Al., L. A. Edwards, E. Al., O.
307   J. Becher, E. Al., V. Clement, E. Al., H. Kettenmann, E. Al., M. Sielska, E. Al., E. Y. Lin, E.
308   Al., S. J. Coniglio, E. Al., S. Sarkar, E. Al., A. Wu, E. Al., A. Müller, E. Al., H. S. Venkatesh,
309   E. Al., H. Sontheimer, M. H. Cohen, E. Al., P. S. LaViolette, E. Al., M. R. Gilbert, E. Al., T.
310   Sandmann, E. Al., C. Lu-Emerson, E. Al., L. B. Rivera, G. Bergers, G. Bergers, D. Hanahan,
311   K. V. Lu, G. Bergers, E. R. Gerstner, E. Al., E. R. Gerstner, E. Al., Y. Piao, E. Al., L. B. Rivera,

31

312 E. Al., F. Shojaei, N. Ferrara, L. Zhang, E. Al., F. Hu, E. Al., S. M. Pyonteck, E. Al., N.
313 Butowski, E. Al., S. J. Kim, E. Al., P. C. Nowell, M. R. Stratton, E. Al., R. Daneman, E. Al.,
314 Glioblastoma: Defining Tumor Niches. *Trends Cancer* **1**, 252–265 (2015).

315 22. D. F. Quail, J. A. Joyce, The microenvironmental landscape of brain tumors. *Cancer Cell*
316 **31**, 326–341 (2017).

317 23. D. Bayik, J. D. Lathia, Cancer stem cell-immune cell crosstalk in tumour progression.
318 *Nat. Rev. Cancer* **21**, 526–536 (2021).

319 24. S. L. N. Maas, E. R. Abels, L. L. Van De Haar, X. Zhang, L. Morsett, S. Sil, J. Guedes,
320 P. Sen, S. Prabhakar, S. E. Hickman, C. P. Lai, D. T. Ting, X. O. Breakefield, M. L. D.
321 Broekman, J. El Khoury, Glioblastoma hijacks microglial gene expression to support tumor
322 growth. *J. Neuroinflammation* **17**, 1–18 (2020).

323 25. N. Charles, E. C. Holland, The perivascular niche microenvironment in brain tumor
324 progression. *Cell Cycle* **9**, 3012 (2010).

325 26. V. Venkataramani, M. Schneider, F. A. Giordano, T. Kuner, W. Wick, U. Herrlinger, F.
326 Winkler, Disconnecting multicellular networks in brain tumours. *Nat. Rev. Cancer* **22**, 481–
327 491 (2022).

328 27. Y. Pan, M. Monje, Neuron-glial interactions in health and brain cancer. *Adv. Biol.* **6**,
329 e2200122 (2022).

330 28. C. Anastasaki, Y. Gao, D. H. Gutmann, Neurons as stromal drivers of nervous system
331 cancer formation and progression. *Dev. Cell* **58**, 81–93 (2023).

332 29. H. S. Venkatesh, W. Morishita, A. C. Geraghty, D. Silverbush, S. M. Gillespie, M. Arzt,
333 L. T. Tam, C. Espenel, A. Ponnuswami, L. Ni, P. J. Woo, K. R. Taylor, A. Agarwal, A. Regev,
334 D. Brang, H. Vogel, S. Hervey-Jumper, D. E. Bergles, M. L. Suvà, R. C. Malenka, M. Monje,
335 Electrical and synaptic integration of glioma into neural circuits. *Nature* **573**, 539–545 (2019).

336 30. D. Wasilewski, N. Priego, C. Fustero-Torre, M. Valiente, Reactive Astrocytes in Brain
337 Metastasis. *Front. Oncol.* **7** (2017).

338 31. E. Parmigiani, M. Scalera, E. Mori, E. Tantillo, E. Vannini, Old Stars and New Players
339 in the Brain Tumor Microenvironment. *Front. Cell. Neurosci.* **15**, 340 (2021).

340 32. A. Shabtay-Orbach, M. Amit, Y. Binenbaum, S. Na'Ara, Z. Gil, Paracrine regulation of
341 glioma cells invasion by astrocytes is mediated by glial-derived neurotrophic factor. *Int. J.*
342 *Cancer* **137**, 1012–1020 (2015).

343 33. D. Henrik Heiland, V. M. Ravi, S. P. Behringer, J. H. Frenking, J. Wurm, K. Joseph, N.
344 W. C. Garrelfs, J. Strähle, S. Heynckes, J. Grauvogel, P. Franco, I. Mader, M. Schneider, A.-L.
345 Potthoff, D. Delev, U. G. Hofmann, C. Fung, J. Beck, R. Sankowski, M. Prinz, O. Schnell,
346 Tumor-associated reactive astrocytes aid the evolution of immunosuppressive environment in
347 glioblastoma. *Nat. Commun.* **10**, 2541 (2019).

348 34. A. Mega, M. Hartmark Nilsen, L. W. Leiss, N. P. Tobin, H. Miletic, L. Sleire, C. Strell,
349 S. Nelander, C. Krona, D. Hägerstrand, P. Ø. Enger, M. Nistér, A. Östman, Astrocytes enhance
350 glioblastoma growth. *Glia* **68**, 316–327 (2020).

351   35.   M. Valiente, A. C. Obenauf, X. Jin, Q. Chen, X. H.-F. Zhang, D. J. Lee, J. E. Chaft, M.
352   G. Kris, J. T. Huse, E. Brogi, J. Massagué, Serpins promote cancer cell survival and vascular
353   co-option in brain metastasis. *Cell* **156**, 1002–1016 (2014).

354   36.   L. Leiss, E. Mutlu, A. Øyan, T. Yan, O. Tsinkalovsky, L. Sleire, K. Petersen, M. A.
355   Rahman, M. Johannessen, S. S. Mitra, H. K. Jacobsen, K. M. Talasila, H. Miletic, I. Jonassen,
356   X. Li, N. H. Brons, K.-H. Kalland, J. Wang, P. Ø. Enger, Tumour-associated glial host cells
357   display a stem-like phenotype with a distinct gene expression profile and promote growth of
358   GBM xenografts. *BMC Cancer* **17**, 108 (2017).

359   37.   M. C. Krawczyk, J. R. Haney, L. Pan, C. Caneda, R. R. Khankan, S. D. Reyes, J. W.
360   Chang, M. Morselli, H. V. Vinters, A. C. Wang, I. Cobos, M. J. Gandal, M. Bergsneider, W.
361   Kim, L. M. Liau, W. Yong, A. Jalali, B. Deneen, G. A. Grant, G. W. Mathern, A. Fallah, Y.
362   Zhang, Human Astrocytes Exhibit Tumor Microenvironment-, Age-, and Sex-Related
363   Transcriptomic Signatures. *J. Neurosci.* **42**, 1587–1603 (2022).

364   38.   R. Levayer, Solid stress, competition for space and cancer: The opposing roles of
365   mechanical cell competition in tumour initiation and growth. *Semin. Cancer Biol.* **63**, 69–80
366   (2020).

367   39.   R. Levayer, E. Moreno, Mechanisms of cell competition: themes and variations. *J. Cell
368   Biol.* **200**, 689–698 (2013).

369   40.   G. Morata, P. Ripoll, Minutes: Mutants of Drosophila autonomously affecting cell
370   division rate. *Dev. Biol.* **42**, 211–221 (1975).

371   41.   B. Cong, R. L. Cagan, Cell competition and cancer from Drosophila to mammals.
372   *Oncogenesis* **13**, 1–7 (2024).

373   42.   S. J. E. Suijkerbuijk, G. Kolahgar, I. Kucinski, E. Piddini, Cell Competition Drives the
374   Growth of Intestinal Adenomas in Drosophila. *Curr. Biol.* **26**, 428–438 (2016).

375   43.   E. Madan, C. J. Pelham, M. Nagane, T. M. Parker, R. Canas-Marques, K. Fazio, K. Shaik,
376   Y. Yuan, V. Henriques, A. Galzerano, T. Yamashita, M. A. F. Pinto, A. M. Palma, D. Camacho,
377   A. Vieira, D. Soldini, H. Nakshatri, S. R. Post, C. Rhiner, H. Yamashita, D. Accardi, L. A.
378   Hansen, C. Carvalho, A. L. Beltran, P. Kuppusamy, R. Gogna, E. Moreno, Flower isoforms
379   promote competitive growth in cancer. *Nature* **572**, 260–264 (2019).

380   44.   A. Krotenberg Garcia, A. Fumagalli, H. Q. Le, R. Jackstadt, T. R. M. Lannagan, O. J.
381   Sansom, J. van Rheenen, S. J. E. Suijkerbuijk, Active elimination of intestinal cells drives
382   oncogenic growth in organoids. *Cell Rep.* **36**, 109307 (2021).

383   45.   D. J. Flanagan, N. Pentinmikko, K. Luopajärvi, N. J. Willis, K. Gilroy, A. P. Raven, L.
384   Mcgarry, J. I. Englund, A. T. Webb, S. Scharaw, N. Nasreddin, M. C. Hodder, R. A. Ridgway,
385   E. Minnee, N. Sphyris, E. Gilchrist, A. K. Najumudeen, B. Romagnolo, C. Perret, A. C.
386   Williams, H. Clevers, P. Nummela, M. Lähde, K. Alitalo, V. Hietakangas, A. Hedley, W. Clark,
387   C. Nixon, K. Kirschner, E. Y. Jones, A. Ristimäki, S. J. Leedham, P. V. Fish, J.-P. Vincent, P.
388   Katajisto, O. J. Sansom, NOTUM from Apc-mutant cells biases clonal competition to initiate
389   cancer. *Nature* **594**, 430–435 (2021).

390   46.   S. M. van Neerven, N. E. de Groot, L. E. Nijman, B. P. Scicluna, M. S. van Driel, M. C.
391   Lecca, D. O. Warmerdam, V. Kakkar, L. F. Moreno, F. A. Vieira Braga, D. R. Sanches, P.

Ramesh, S. ten Hoorn, A. S. Aelvoet, M. F. van Boxel, L. Koens, P. M. Krawczyk, J. Koster, E. Dekker, J. P. Medema, D. J. Winton, M. F. Bijlsma, E. Morrissey, N. Léveillé, L. Vermeulen, Apc-mutant cells act as supercompetitors in intestinal tumour initiation. *Nature* **594**, 436–441 (2021).

47.   M. Vishwakarma, E. Piddini, Outcompeting cancer. *Nat. Rev. Cancer* **20**, 187–198 (2020).

48.   D. Yang, W. Sun, L. Gao, K. Zhao, Q. Zhuang, Y. Cai, Cell competition as an emerging mechanism and therapeutic target in cancer. *Biochim. Biophys. Acta BBA - Mol. Basis Dis.* **1871**, 167769 (2025).

49.   S. M. van Neerven, L. Vermeulen, Cell competition in development, homeostasis and cancer. *Nat. Rev. Mol. Cell Biol.* **24**, 221–236 (2023).

50.   D. Ceresa, F. Alessandrini, S. Lucchini, D. Marubbi, F. Piaggio, J. M. Mena Vera, I. Ceccherini, D. Reverberi, I. Appolloni, P. Malatesta, Early clonal extinction in glioblastoma progression revealed by genetic barcoding. *Cancer Cell* **41**, 1466-1479.e9 (2023).

51.   G. Seano, H. T. Nia, K. E. Emblem, M. Datta, J. Ren, S. Krishnan, J. Kloepper, M. C. Pinho, W. W. Ho, M. Ghosh, V. Askoxylakis, G. B. Ferraro, L. Riedemann, E. R. Gerstner, T. T. Batchelor, P. Y. Wen, N. U. Lin, A. J. Grodzinsky, D. Fukumura, P. Huang, J. W. Baish, T. P. Padera, L. L. Munn, R. K. Jain, Solid stress in brain tumours causes neuronal loss and neurological dysfunction and can be reversed by lithium. *Nat. Biomed. Eng. 2019 33* **3**, 230–245 (2019).

52.   V. Labi, M. Erlacher, How cell death shapes cancer. *Cell Death Dis.* **6**, e1675–e1675 (2015).

53.   G. Ichim, S. W. G. Tait, A fate worse than death: apoptosis as an oncogenic process. *Nat. Rev. Cancer* **16**, 539–548 (2016).

54.   O. Morana, W. Wood, C. D. Gregory, The Apoptosis Paradox in Cancer. *Int. J. Mol. Sci.* **23**, 1328 (2022).

55.   M.-C. Fitzgerald, P. J. O'Halloran, N. M. C. Connolly, B. M. Murphy, Targeting the apoptosis pathway to treat tumours of the paediatric nervous system. *Cell Death Dis.* **13**, 1–10 (2022).

56.   K. Malone, E. LaCasse, S. T. Beug, Cell death in glioblastoma and the central nervous system. *Cell. Oncol.* **48**, 313–349 (2025).

57.   H. Mira, J. Morante, Neurogenesis From Embryo to Adult – Lessons From Flies and Mice. *Front. Cell Dev. Biol.* **8**, 533 (2020).

58.   Y. Jiang, H. Reichert, Drosophila neural stem cells in brain development and tumor formation. *J. Neurogenet.* **28**, 181–189 (2014).

59.   C. Maurange, Temporal patterning in neural progenitors: from Drosophila development to childhood cancers. *Dis. Model. Mech.* **13** (2020).

429   60.   S. P. Choksi, T. D. Southall, T. Bossing, K. Edoff, E. de Wit, B. E. Fischer, B. van
430   Steensel, G. Micklem, A. H. Brand, Prospero acts as a binary switch between self-renewal and
431   differentiation in Drosophila neural stem cells. *Dev Cell* **11**, 775–789 (2006).

432   61.   K. Narbonne-Reveau, E. Lanet, C. Dillard, S. Foppolo, C. H. Chen, H. Parrinello, S.
433   Rialle, N. S. Sokol, C. Maurange, Neural stem cell-encoded temporal patterning delineates an
434   early window of malignant susceptibility in Drosophila. *eLife* **5**, 1–29 (2016).

435   62.   S. Genovese, R. Clément, C. Gaultier, F. Besse, K. Narbonne-Reveau, F. Daian, S.
436   Foppolo, N. M. Luis, C. Maurange, Coopted temporal patterning governs cellular hierarchy,
437   heterogeneity and metabolism in drosophila Neuroblast tumors. *eLife* **8** (2019).

438   63.   C. Gaultier, S. Foppolo, C. Maurange, Regulation of developmental hierarchy in
439   Drosophila neural stem cell tumors by COMPASS and Polycomb complexes. *Sci. Adv.* **8**
440   (2022).

441   64.   G. F. Valamparamban, P. Spéder, Homemade: building the structure of the neurogenic
442   niche. *Front. Cell Dev. Biol.* **11**, 1275963 (2023).

443   65.   M. R. Freeman, Drosophila Central Nervous System Glia. *Cold Spring Harb. Perspect.*
444   *Biol.* **7** (2015).

445   66.   S. J. Hindle, R. J. Bainton, Barrier mechanisms in the Drosophila blood-brain barrier.
446   *Front. Neurosci.* **8**, 414 (2014).

447   67.   K. Dumstrei, F. Wang, V. Hartenstein, Role of DE-Cadherin in Neuroblast Proliferation,
448   Neural Morphogenesis, and Axon Tract Formation in DrosophilaLarval Brain Development. *J.*
449   *Neurosci.* **23**, 3325 (2003).

450   68.   W. Pereanu, D. Shy, V. Hartenstein, Morphogenesis and proliferation of the larval brain
451   glia in Drosophila. *Dev. Biol.* **283**, 191–203 (2005).

452   69.   J. C. Coutinho-Budd, A. E. Sheehan, M. R. Freeman, The secreted neurotrophin Spätzle
453   3 promotes glial morphogenesis and supports neuronal survival and function. *Genes Dev.* **31**,
454   2023–2038 (2017).

455   70.   M. A. Rujano, D. Briand, B. Đelić, J. Marc, P. Spéder, An interplay between cellular
456   growth and atypical fusion defines morphogenesis of a modular glial niche in Drosophila. *Nat.*
457   *Commun.* **13**, 4999 (2022).

458   71.   V. Yadav, R. Mishra, P. Das, R. Arya, Cut homeodomain transcription factor is a novel
459   regulator of growth and morphogenesis of cortex glia niche around neural cells. *Genetics*, doi:
460   10.1093/GENETICS/IYAD173 (2023).

461   72.   J. Morante, D. M. Vallejo, C. Desplan, M. Dominguez, Conserved miR-8/miR-200
462   defines a glial niche that controls neuroepithelial expansion and neuroblast transition. *Dev. Cell*
463   **27**, 174–187 (2013).

464   73.   A. P. Bailey, G. Koster, C. Guillermier, E. M. A. Hirst, J. I. MacRae, C. P. Lechene, A.
465   D. Postle, A. P. Gould, Antioxidant Role for Lipid Droplets in a Stem Cell Niche of Drosophila.
466   *Cell* **163**, 340–353 (2015).

467 74. Q. Dong, M. Zavortink, F. Froldi, S. Golenkina, T. Lam, L. Y. Cheng, Glial Hedgehog
468 signalling and lipid metabolism regulate neural stem cell proliferation in Drosophila. *EMBO*
469 *Rep.*, doi: 10.15252/embr.202052130 (2021).

470 75. A. de Torres-Jurado, S. Manzanero-Ortiz, A. Carmena, Glial-secreted Netrins regulate
471 Robo1/Rac1-Cdc42 signaling threshold levels during Drosophila asymmetric neural
472 stem/progenitor cell division. *Curr. Biol. CB* **32**, 2174-2188.e3 (2022).

473 76. P. Spéder, A. H. Brand, Systemic and local cues drive neural stem cell niche remodelling
474 during neurogenesis in Drosophila. *eLife* **7**, e30413 (2018).

475 77. H. Plazaola-Sasieta, Q. Zhu, H. Gaitán-Peñas, M. Rios, R. Estévez, M. Morey,
476 Drosophila ClC-a is required in glia of the stem cell niche for proper neurogenesis and wiring
477 of neural circuits. *Glia* **67**, 2374 (2019).

478 78. A. Banach-Latapy, V. Rincheval, D. Briand, I. Guénal, P. Spéder, Differential adhesion
479 during development establishes individual neural stem cell niches and shapes adult behaviour
480 in Drosophila. *PLoS Biol.* **21**, e3002352 (2023).

481 79. M. A. Logan, Glial contributions to neuronal health and disease: new insights from
482 Drosophila. *Curr. Opin. Neurobiol.* **47**, 162–167 (2017).

483 80. G. Artiushin, A. Sehgal, The Glial Perspective on Sleep and Circadian Rhythms. *Annu.*
484 *Rev. Neurosci.* **43**, 119–140 (2020).

485 81. C. Kiyoshi, M. Zhou, Astrocyte syncytium: a functional reticular system in the brain.
486 *Neural Regen. Res.* **14**, 595 (2019).

487 82. C. S. Bjornsson, M. Apostolopoulou, Y. Tian, S. Temple, It Takes a Village: Constructing
488 the Neurogenic Niche. *Dev. Cell* **32**, 435–446 (2015).

489 83. W. Boll, M. Noll, The Drosophila Pox neuro gene: control of male courtship behavior
490 and fertility as revealed by a complete dissection of all enhancers. *Dev. Camb. Engl.* **129**, 5667–
491 5681 (2002).

492 84. O. Kanca, E. Caussinus, A. S. Denes, A. Percival-Smith, M. Affolter, Raeppli: a whole-
493 tissue labeling tool for live imaging of Drosophila development. *Development* **141**, 472–480
494 (2014).

495 85. S. Schott, A. Ambrosini, A. Barbaste, C. Benassayag, M. Gracia, A. Proag, M. Rayer, B.
496 Monier, M. Suzanne, A fluorescent toolkit for spatiotemporal tracking of apoptotic cells in
497 living Drosophila tissues. *Dev. Camb.* **144**, 3840–3846 (2017).

498 86. N. Shinoda, N. Hanawa, T. Chihara, A. Koto, M. Miura, Dronc-independent basal
499 executioner caspase activity sustains Drosophila imaginal tissue growth. *Proc. Natl. Acad. Sci.*
500 **116**, 20539–20544 (2019).

501 87. T. D. Southall, K. S. Gold, B. Egger, C. M. Davidson, E. E. Caygill, O. J. Marshall, A.
502 H. Brand, Cell-type-specific profiling of gene expression and chromatin binding without cell
503 isolation: assaying RNA Pol II occupancy in neural stem cells. *Dev. Cell* **26**, 101–12 (2013).

504   88.   O. J. Marshall, T. D. Southall, S. W. Cheetham, A. H. Brand, Cell-type-specific profiling
505   of protein–DNA interactions without cell isolation using targeted DamID with next-generation
506   sequencing. *Nat. Protoc.* **11**, 1586–1598 (2016).

507   89.   D. N. Dhanasekaran, E. Premkumar Reddy, JNK-signaling: A multiplexing hub in
508   programmed cell death. *Genes Cancer* **8**, 682 (2017).

509   90.   G. Nadel, G. Maik-Rachline, R. Seger, JNK Cascade-Induced Apoptosis—A Unique
510   Role in GqPCR Signaling. *Int. J. Mol. Sci.* **24**, 13527 (2023).

511   91.   E. F. Wagner, A. R. Nebreda, Signal integration by JNK and p38 MAPK pathways in
512   cancer development. *Nat. Rev. Cancer* **9**, 537–549 (2009).

513   92.   F. Chen, JNK-induced apoptosis, compensatory growth, and cancer stem cells. *Cancer*
514   *Res.* **72**, 379–386 (2012).

515   93.   C. Tournier, The 2 Faces of JNK Signaling in Cancer. *Genes Cancer* **4**, 397–400 (2013).

516   94.   S. Y. Tam, H. K.-W. Law, JNK in Tumor Microenvironment: Present Findings and
517   Challenges in Clinical Translation. *Cancers* **13**, 2196 (2021).

518   95.   G. S. Hotamisligil, R. J. Davis, Cell Signaling and Stress Responses. *Cold Spring Harb.*
519   *Perspect. Biol.* **8**, a006072 (2016).

520   96.   B. Glise, H. Bourbon, S. Noselli, hemipterous encodes a novel Drosophila MAP kinase
521   kinase, required for epithelial cell sheet movement. *Cell* **83**, 451–461 (1995).

522   97.   E. Martín-Blanco, A. Gampel, J. Ring, K. Virdee, N. Kirov, A. M. Tolkovsky, A.
523   Martinez-Arias, puckered encodes a phosphatase that mediates a feedback loop regulating JNK
524   activity during dorsal closure in Drosophila. *Genes Dev.* **12**, 557–570 (1998).

525   98.   J. M. Ring, A. Martinez Arias, puckered, a gene involved in position-specific cell
526   differentiation in the dorsal epidermis of the Drosophila larva. *Dev. Camb. Engl. Suppl.*, 251–
527   259 (1993).

528   99.   H. Kanda, T. Igaki, Mechanism of tumor-suppressive cell competition in flies. *Cancer*
529   *Sci.* **111**, 3409–3415 (2020).

530   100.   Bergmann, A, Cell Death, Compensatory Proliferation, and Cell Competition. *Annu. Rev.*
531   *Genet.*, doi: 10.1146/annurev-genet-012125-083359 (2025).

532   101.   S. E. McGuire, P. T. Le, A. J. Osborn, K. Matsumoto, R. L. Davis, Spatiotemporal rescue
533   of memory dysfunction in Drosophila. *Science* **302**, 1765–8 (2003).

534   102.   A. M. Brumby, H. E. Richardson, scribble mutants cooperate with oncogenic Ras or
535   Notch to cause neoplastic overgrowth in Drosophila. *EMBO J.* **22**, 5769–5779 (2003).

536   103.   T. Igaki, J. C. Pastor-Pareja, H. Aonuma, M. Miura, T. Xu, Intrinsic tumor suppression
537   and epithelial maintenance by endocytic activation of Eiger/TNF signaling in Drosophila. *Dev.*
538   *Cell* **16**, 458–465 (2009).

539   104. C. de la Cova, M. Abril, P. Bellosta, P. Gallant, L. A. Johnston, Drosophila myc regulates
540   organ size by inducing cell competition. *Cell* **117**, 107–116 (2004).

541   105. E. Moreno, K. Basler, dMyc transforms cells into super-competitors. *Cell* **117**, 117–129
542   (2004).

543   106. N. Pinal, M. Calleja, G. Morata, Pro-apoptotic and pro-proliferation functions of the JNK
544   pathway of Drosophila: roles in cell competition, tumorigenesis and regeneration. *Open Biol.*
545   **9**, 180256 (2019).

546   107. J. E. La Marca, H. E. Richardson, Two-Faced: Roles of JNK Signalling During
547   Tumourigenesis in the Drosophila Model. *Front. Cell Dev. Biol.* **8**, 511771 (2020).

548   108. B. Mollereau, A. Perez-Garijo, A. Bergmann, M. Miura, O. Gerlitz, H. D. Ryoo, H.
549   Steller, G. Morata, Compensatory proliferation and apoptosis-induced proliferation: a need for
550   clarification. *Cell Death Differ.* **20**, 181–181 (2013).

551   109. J. P. Parvy, Y. Yu, A. Dostalova, S. Kondo, A. Kurjan, P. Bulet, B. Lemaître, M. Vidal,
552   J. B. Cordero, The antimicrobial peptide defensin cooperates with tumour necrosis factor to
553   drive tumour cell death in Drosophila. *eLife* **8** (2019).

554   110. S. N. Meyer, M. Amoyel, C. Bergantiños, C. de la Cova, C. Schertel, K. Basler, L. A.
555   Johnston, An ancient defense system eliminates unfit cells from developing tissues during cell
556   competition. *Science* **346**, 1258236 (2014).

557   111. R. D. Read, W. K. Cavenee, F. B. Furnari, J. B. Thomas, A drosophila model for EGFR-
558   Ras and PI3K-dependent human glioma. *PLoS Genet.* **5**, e1000374 (2009).

559   112. M. Portela, V. Venkataramani, N. Fahey-Lozano, E. Seco, M. Losada-Perez, F. Winkler,
560   S. Casas-Tintó, Glioblastoma cells vampirize WNT from neurons and trigger a JNK/MMP
561   signaling loop that enhances glioblastoma progression and neurodegeneration. *PLoS Biol.* **17**
562   (2019).

563   113. J. Shklover, K. Mishnaevski, F. Levy-Adam, E. Kurant, JNK pathway activation is able
564   to synchronize neuronal death and glial phagocytosis in Drosophila. *Cell Death Dis.* **6**, e1649
565   (2015).

566   114. R. Hilu-Dadia, K. Hakim-Mishnaevski, F. Levy-Adam, E. Kurant, Draper-mediated JNK
567   signaling is required for glial phagocytosis of apoptotic neurons during Drosophila
568   metamorphosis. *Glia* **66**, 1520–1532 (2018).

569   115. A. Matamoro-Vidal, T. Cumming, A. Davidović, F. Levillayer, R. Levayer, Patterned
570   apoptosis has an instructive role for local growth and tissue shape regulation in a fast-growing
571   epithelium. *Curr. Biol.* **34**, 376-388.e7 (2024).

572   116. A. Pérez-Garijo, Y. Fuchs, H. Steller, Apoptotic cells can induce non-autonomous
573   apoptosis through the TNF pathway. *eLife* **2**, e01004 (2013).

574   117. L. K. Petersen, R. S. Stowers, A Gateway MultiSite recombination cloning toolkit. *PloS*
575   *One* **6**, e24531 (2011).

576 118. O. J. Marshall, A. H. Brand, damidseq_pipeline: an automated pipeline for processing
577 DamID sequencing datasets. *Bioinforma. Oxf. Engl.* **31**, 3371–3 (2015).

578 119. O. Marshall, owenjm/polii.gene.call, (2020); https://github.com/owenjm/polii.gene.call.

579 120. S. Tarazona, P. Furió-Tarí, D. Turrà, A. D. Pietro, M. J. Nueda, A. Ferrer, A. Conesa,
580 Data quality aware analysis of differential expression in RNA-seq with NOISeq R/Bioc
581 package. *Nucleic Acids Res.* **43**, e140 (2015).

582 121. B. T. Sherman, M. Hao, J. Qiu, X. Jiao, M. W. Baseler, H. C. Lane, T. Imamichi, W.
583 Chang, DAVID: a web server for functional enrichment analysis and functional annotation of
584 gene lists (2021 update). *Nucleic Acids Res.* **50**, W216–W221 (2022).

585 122. R: The R Project for Statistical Computing. https://www.r-project.org/.

586 123. M. Tennekes, P. Ellis, treemap: Treemap Visualization, version 2.4-4 (2023);
587 https://cran.r-project.org/web/packages/treemap/index.html.

588 124. R. Kolde, pheatmap: Pretty Heatmaps, version 1.0.13 (2025); https://cran.r-
589 project.org/web/packages/pheatmap/index.html.

590 125. W. Luo, C. Brouwer, Pathview: an R/Bioconductor package for pathway-based data
591 integration and visualization. *Bioinformatics* **29**, 1830–1831 (2013).

592

Main Figures and Captions for

Cell competition overcomes host tissue resistance to unleash tumour growth in a *Drosophila* brain cancer model

Gualtieri et al

Figure 1

A. NSC → GMC → Neuron; pros⁻; CSC / CPC / CPC with Dpn, Imp, Chinmo, Lin-28, Syncrip, E93, Cdc25, E(spl)/Hes; self-renewal

B. Poxn tumours (6 clusters); Day 1, Day 3, Day 6, Day 9; Dpn (CSPC); 20 µm scale bars

C. Tumour volume (µm³) x10⁶; Day 1 (n = 5), Day 3 (n = 8), Day 6 (n = 6), Day 9 (n = 3); 0.0064, 0.0417, 0.0003

D. Larva L3; 10 µm; Dpn (NSC) ElaV (Neurons) Nrv2::GFP (CG membrane)

E. CG, NSC, GMC, Neuron

F. Day 3; 10 µm

G. CG, Neuron

H. Larva L3; Day 1; Day 3; Day 6; Day 9; 10 µm; Dpn (CSPC) ElaV (Neurons) Nrv2::GFP (CG membrane)

I. CG membrane volume to Tumour Volume (%); Day 1 (n = 5), Day 3 (n = 6), Day 6 (n = 5), Day 9 (n = 7); >0.9999, 0.4859, >0.9999, 0.0008

J. poxn > prosRNAi, RAEPPLI-NLS; LARVA L3; Stochastic induction and labelling; Clonal labelling; ADULT?

K. Larva L3; Day 1; Day 6; 10 µm; RAEPPLI-NLS (CSPC) Nrv2::GFP (CG membrane)
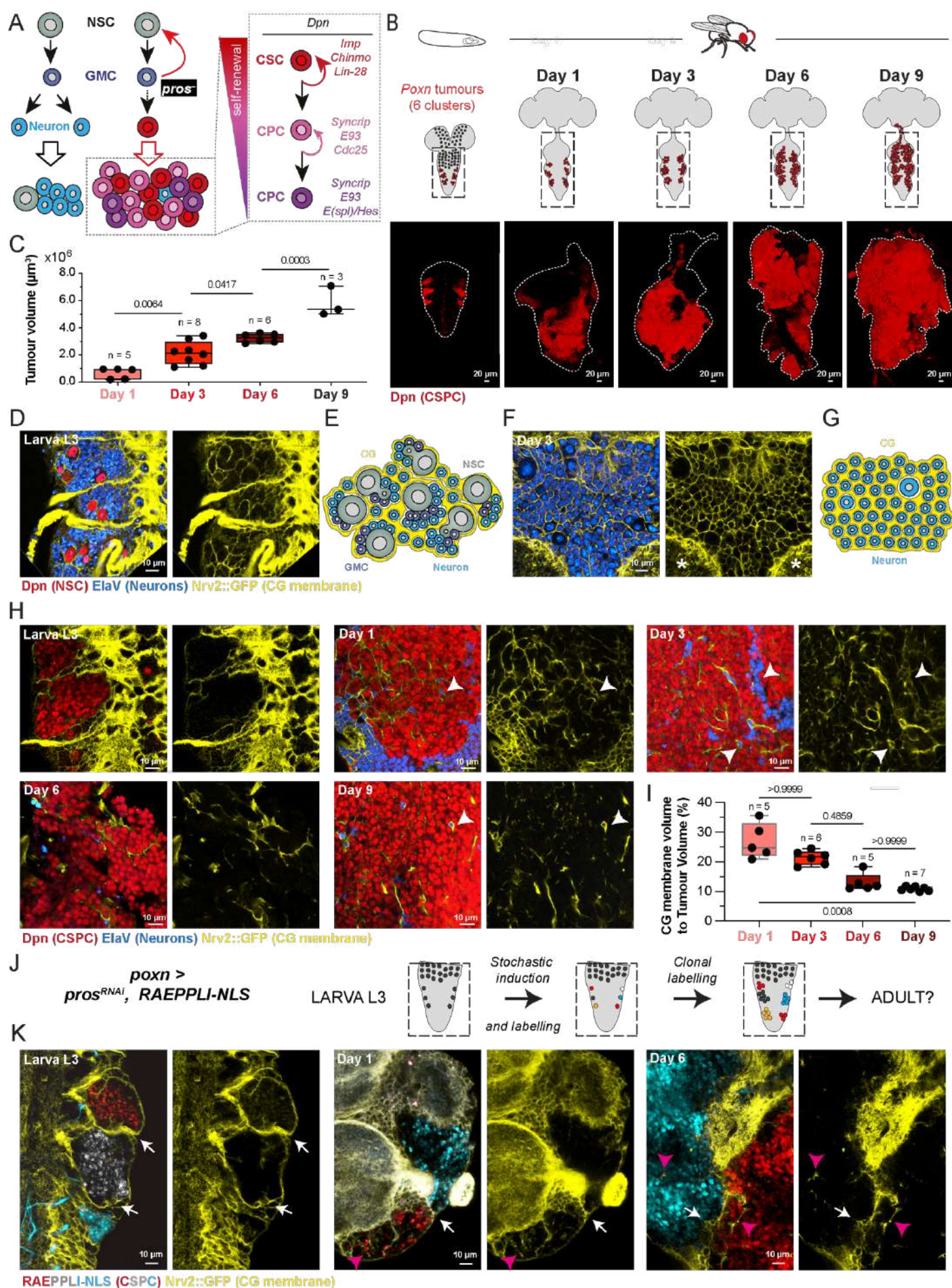
2

Figure 1. Cancer stem cell-driven tumours remodel the host glial microenvironment

(**A**) Schematic of tumour initiation from transformed neural stem cells. During normal larval neurogenesis, neural stem cells (NSCs, grey) divide asymmetrically to generate one ganglion mother cell (GMC, purple), a precursor which will divide further only once in a symmetric fashion to produce two neurons (N, blue, depicted here) or more rarely glial cells. Upon the loss of *prospero* (*pros*), a gene driving NSC differentiation, GMCs revert to a stem cell-like fate, transforming into Cancer Stem Cells (CSCs, red). These CSCs (marked by the expression of Imp, Chinmo and Lin-28) are at the apex of the cellular hierarchy (insert). They will generate the diversity of the tumour, composed of CSCs and Cancer Progenitors Cells (CPCs, in pink and purple shades) of varied potential (marked by Syncrip and E93, and differentiated by the expression of Cdc25 or E(spl)/Hes), and occasionally neurons. All CSCs and CPCs (collectively refered as to CSPCs) express the transcription factor Deadpan (Dpn).

(**B**) Schematic and illustration of tumour growth in $pros^{poxn}$ tumours (*poxn* > $pros^{RNAi}$). Six individual tumours are initiated at the larval stage by the specific knockdown of *pros* in the six Poxn$^+$ NSCs located in the ventral nerve cord (VNC, highlighted in dashed black rectangles), in a dorsal and posterior thoracic fashion, using a restricted GAL4 driver (*poxn-GAL4*). Shortly after adult eclosion (day 0), the tumours have started growing (day 1) and they will keep expanding towards the central brain until around day 9 where the flies die. Confocal pictures are 3D reconstructions of tumours stained with Deadpan (Dpn, red), a marker of NSCs and CSCs. Dashed white lines delineate the VNC.

(**C**) Quantification of tumour volume over time. n = VNC. One-way ANOVA with Tukey's multiple comparison tests.

(**D**) Confocal image showing the NSC niche at third larval stage (L3), in which Poxn$^+$ NSCs transform into CSCs upon *pros* knockdown. NSCs and their neuronal progeny are closely enwrapped by cortex glia (CG) membranes.

(**E**) Schematic of the NSC niche at larval stage.

(**F**) Confocal image showing the host cellular microenvironment, in which the CSC-driven tumour will expand, at adult stage. Neurons are surrounded by a tight meshwork of CG membranes. Neuropile structures, in which synapses form, are indicated by white stars.

(**G**) Schematic of the host cellular microenvironment at adult stage

(**H**) Crops of confocal images illustrating the progressive remodelling of CG membranes in the VNC upon tumour progression. White arrowheads indicate examples of individually enwrapped neurons.

34   (**I**) Quantification of CG membranes volume compared to tumour volume along tumour

35   progression. n = tumour. Kruskal–Wallis H test with Dunn's multiple comparisons test.

36   (**J**) Principle of clonal tumour labeling using the genetic construct Raeppli-NLS. Early

37   induction by heatshock at larval stage leads to the labelling of each of the six original Poxn[+]

38   CSCs by one out of four possible colour choices. The entire lineage of each CSC will inherit

39   the colour which will be genetically maintained over the entire lifespan, thus allowing the

40   tracking of the six individual tumours within the CNS.

41   (**K**) Confocal images of *pros^{poxn}* tumours labelled by Raeppli-NLS within the CG membrane

42   (yellow) at third larval stage (L3) and days 1 and 6 of adulthood. While the CG remodels, the

43   entire tumour lineages keep together and stay separated from one another by a layer of CG

44   membranes, similarly to larval NSC lineages. White arrows show the location of the CG

45   separating tumour clones. Pink arrowheads indicate examples of CG membranes infiltrating

46   within the tumour mass.

47

48

49   For box plots, individual values are superimposed.

50   See also Table S1.

51 **Figure 2**

Dpn (CSPC) ElaV (Neurons) Repo (glia nuclei)
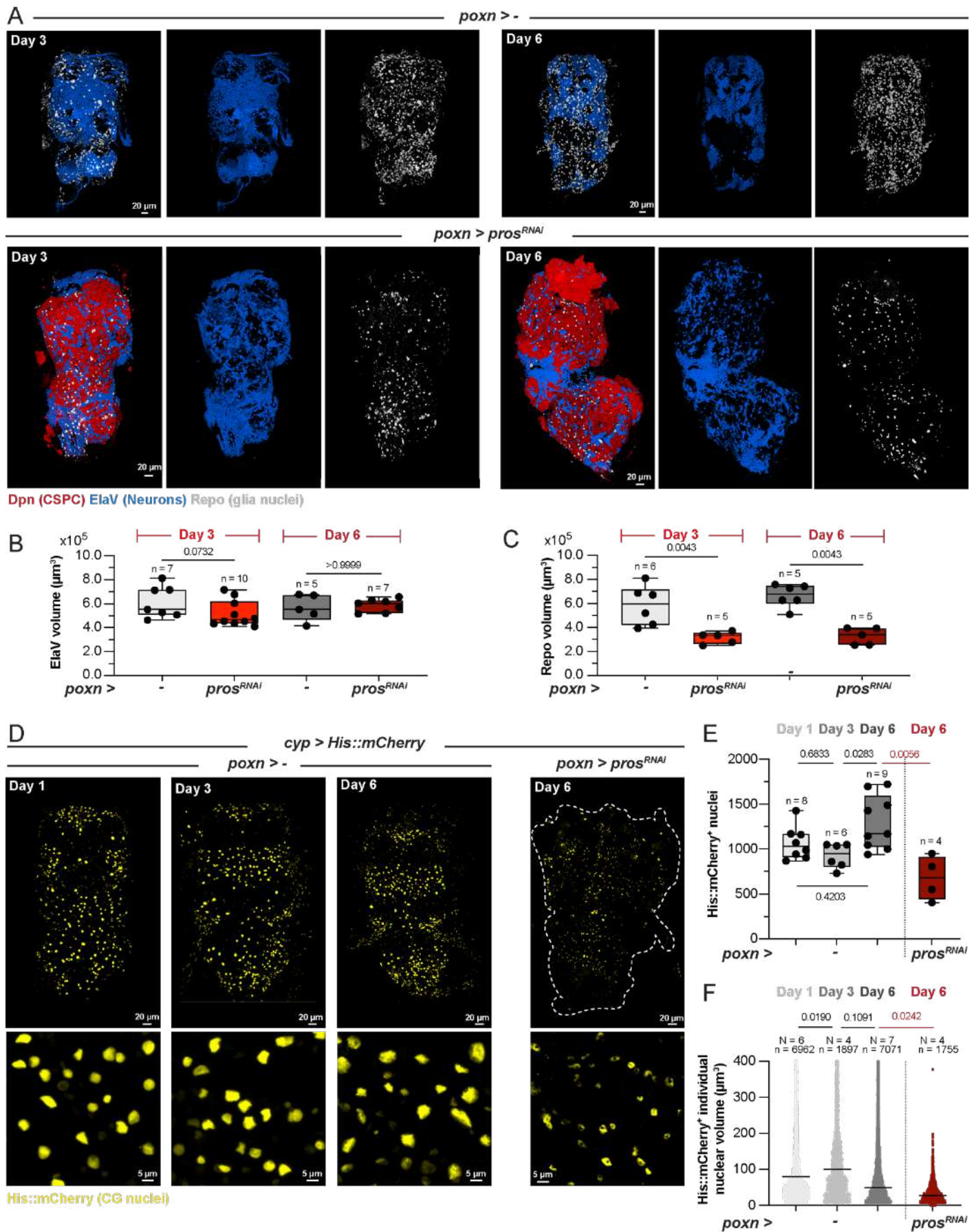
His::mCherry (CG nuclei)

1   **Figure 2. Cortex glia, but not neurons, are lost upon tumour progression**

2   (**A**) 3D reconstruction of confocal images showing whole VNCs stained for neuronal (ElaV,

3   blue) and glial (Repo, gray) nuclei for control (*poxn* > -) and *pros^{poxn}* tumour conditions (*poxn*

4   > *pros^{RNAi}*) at days 3 and 6 of adulthood.

5   (**B**) Box plot of total neuron (ElaV$^+$) volume for control (*poxn* > -) and *pros^{poxn}* tumour

6   conditions (*poxn* > *pros^{RNAi}*) at days 3 and 6 of adulthood. n = VNC. Mann-Whitney U tests for

7   each day.

8   (**C**) Box plot of total glia (Repo$^+$) volume for control (*poxn* > -) and *pros^{poxn}* tumour conditions

9   (*poxn* > *pros^{RNAi}*) at days 3 and 6 of adulthood. n = VNC. Mann-Whitney U tests for each day.

10   (**D**) Confocal images of CG nuclei genetically labelled by a His::mCherry fusion (*cyp* >

11   *His::mCherry*, yellow) for control (*poxn* > -) for days 1, 3 and 6 of adulthood and *pros^{poxn}*

12   tumour conditions (*poxn* > *pros^{RNAi}*) for day 6 of adulthood. Upper panels show 3D

13   reconstruction of whole VNCs and lower panels show a close-up projection.

14   (**E**) Box plot of CG nuclei number for control (*poxn* > -) at days 1, 3 and 6 of adulthood and

15   *pros^{poxn}* tumour conditions (*poxn* > *pros^{RNAi}*) at day 6 of adulthood. n = VNC. One-way

16   ANOVA with Tukey's multiple comparisons test between the control conditions. Mann-

17   Whitney U tests between chosen pairs.

18   (**F**) Dot plot of CG individual nuclear volume for control (*poxn* > -) at days 1, 3 and 6 of

19   adulthood and *pros^{poxn}* tumour conditions (*poxn* > *pros^{RNAi}*) at day 6 of adulthood. Dot = CG

20   nucleus. N = VNC. n = CG nucleus. Mann-Whitney U tests between chosen pairs were

21   performed on the mean values per VNC.

22

23   For box plots, individual values are superimposed.

24   See also Table S1.

6

Figure 3

Dpn (CSPC) GC3Ai (apoptotic marker)

Dpn (CSPC) ElaV (Neurons) Repo (glia nuclei)
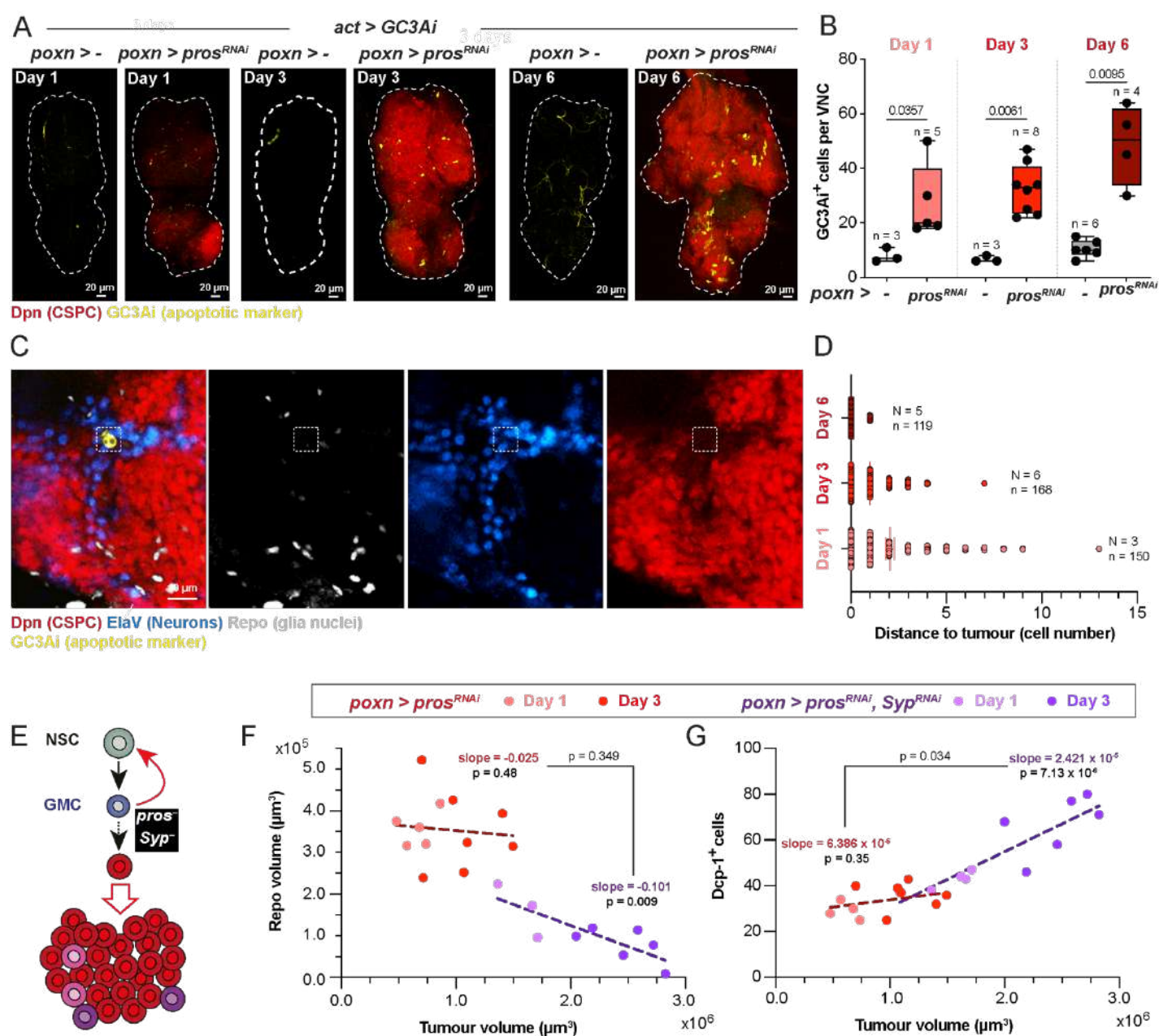GC3Ai (apoptotic marker)

1 **Figure 3. Glia, including the cortex glia, undergo cancer stem cell-driven apoptosis**

2 (**A**) 3D reconstruction of confocal images showing whole VNCs stained for tumour (Dpn, red)

3 and for a genetic reporter of apoptosis (GC3Ai, yellow) for control (*poxn* > -) and *pros^poxn*

4 tumour conditions (*poxn* > *pros^{RNAi}*) at days 1, 3 and 6 of adulthood.

5 (**B**) Box plot of GC3Ai$^+$ cells per VNC for control (*poxn* > -) and *pros^poxn* tumour conditions

6 (*poxn* > *pros^{RNAi}*) at days 1, 3 and 6 of adulthood. n = VNC. Mann-Whitney U tests for each

7 day.

8 (**C**) Confocal close-up image illustrating the localisation of one apoptotic cell (dashed box),

9 marked by GC3Ai, compared to the tumour edge. This cell has already lost its identity marker,

10 and does not co-stain for glia (Repo) or neuron (ElaV) marker.

11 (**D**) Dot plot of the number of cells between GC3Ai$^+$ cells and the tumour edge at days 1, 3 and

12 6 of adulthood. Dot = GC3Ai$^+$ cells. N = VNC. n = GC3Ai$^+$ cells.

13 (**E**) Schematic of tumour initiation from transformed neural stem cells upon the combined loss

14 of *prospero* (*pros*) and *Syncrip* (*Syp*). These tumours (*Syp^{RNAi}, pros^poxn*) are nearly exclusively

15 composed of CSCs (Imp$^+$, Chinmo$^+$ and Lin-28$^+$).

16 (**F**) Scatterplot and linear regression analysis of glial volume *versus* tumour volume for *pros^poxn*

17 tumours (*poxn* > *pros^{RNAi}*) and *Syp^{RNAi}, pros^poxn* (*poxn* > *pros^{RNAi}, Syp^{RNAi}*) tumours. Each dot

18 represents a VNC. 12 VNCs were used for *pros^poxn* tumours and 9 VNCs were used for *Syp^{RNAi},*

19 *pros^poxn* tumours to plot the respective linear regression (dotted lines). A linear model was used

20 to calculate the p-values for each linear regression (giving the significance of correlation), and

21 for the difference between the two linear regressions.

22 (**G**) Scatterplot and linear regression analysis of apoptotic cell counts *versus* tumour volume

23 for *pros^poxn* tumours and *Syp^{RNAi}, pros^poxn* tumours. Each dot represents a VNC. 11 VNCs were

24 used for *pros^poxn* tumours and 11 VNCs were used for *Syp^{RNAi}, pros^poxn* tumours to plot the

25 respective linear regression (dotted lines). A linear model was used to calculate the p-values for

26 each linear regression (giving the significance of correlation), and for the difference between

27 the two linear regressions.

28

29

30 For box plots, individual values are superimposed.

31 See also Table S1

Figure 4

Figure 4. Panel A: poxn > pros^RNAi, cyp > - and poxn > pros^RNAi, cyp > reaper, Day 3 and Day 6. Dpn (CSPC) Dcp-1 (apoptotic marker). Panel D: poxn > pros^RNAi, cyp > - and poxn > pros^RNAi, cyp > p35, Day 6. Dpn (CSPC) Repo (glia nuclei). Panels B, C, E, F show quantification box plots.
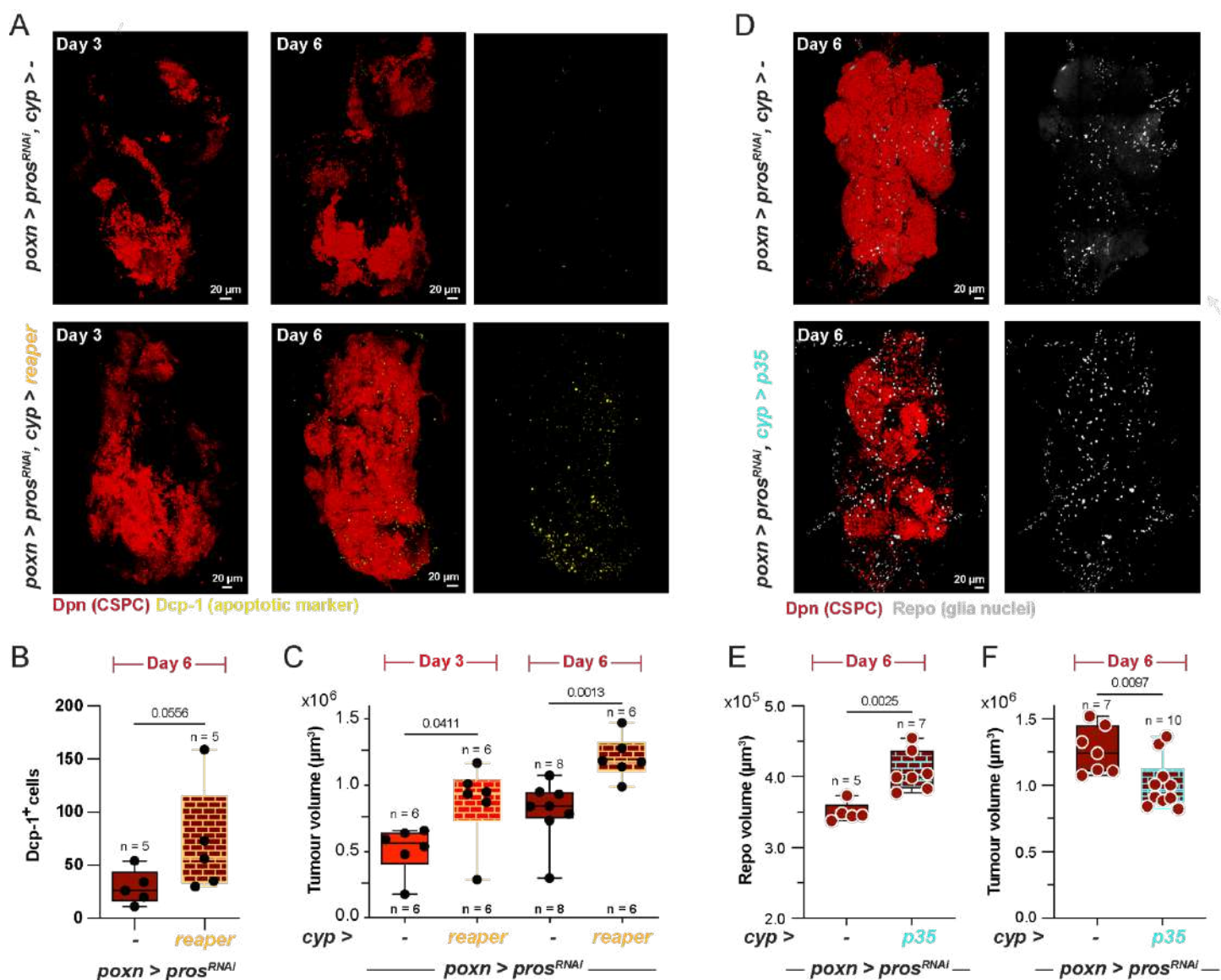
1   **Figure 4. Cortex glia apoptosis promotes tumour growth and its prevention reveals a**

2   **capacity of resistance from the host tissue**

3   (**A**) 3D reconstruction of confocal images showing whole VNCs stained for tumour (Dpn, red)

4   and for apoptotic cells (Dcp-1, yellow) for control tumours (*poxn > pros^{RNAi}, cyp > -*) and

5   tumours in which apoptosis has been induced from day 0 in all CG cells through the specific

6   expression of the pro-apoptotic gene *reaper* (*poxn > pros^{RNAi}, cyp > reaper*) at days 3 and 6 of

7   adulthood.

8   (**B**) Box plot of apoptotic (Dcp-1^{+}) cells numbers per VNC for (*poxn > pros^{RNAi}, cyp > -*) and

9   (*poxn > pros^{RNAi}, cyp > reaper*) tumour conditions at day 6 of adulthood. n = VNC. Mann-

10   Whitney U test.

11   (**C**) Box plot of tumour volume for (*poxn > pros^{RNAi}, cyp > -*) and (*poxn > pros^{RNAi}, cyp >*

12   *reaper*) tumour conditions at days 3 and 6 of adulthood. n = VNC. Mann-Whitney U tests for

13   each day.

14   (**D**) 3D reconstruction of confocal images showing whole VNCs stained for tumour (Dpn, red)

15   and for glial cells (Repo, yellow) for control tumours (*poxn > pros^{RNAi}, cyp > -*) and tumours in

16   which apoptosis has been blocked from day 0 in all CG cells through the specific expression of

17   the anti-apoptotic exogenous gene *p35* (*poxn > pros^{RNAi}, cyp > p35*) at day 6 of adulthood.

18   (**E**) Box plot of total glial nuclear (Repo) volume for (*poxn > pros^{RNAi}, cyp > -*) and (*poxn >*

19   *pros^{RNAi}, cyp > p35*) tumour conditions at day 6 of adulthood. n = VNC. Mann-Whitney U test.

20   (**F**) Box plot of tumour volume for (*poxn > pros^{RNAi}, cyp > -*) and (*poxn > pros^{RNAi}, cyp > p35*)

21   tumour conditions at day 6 of adulthood. n = VNC. Mann-Whitney U test.

22

23

24   For box plots, individual values are superimposed.

25   See also Table S1.

Figure 5

A cyp > Dam / Dam-PolII

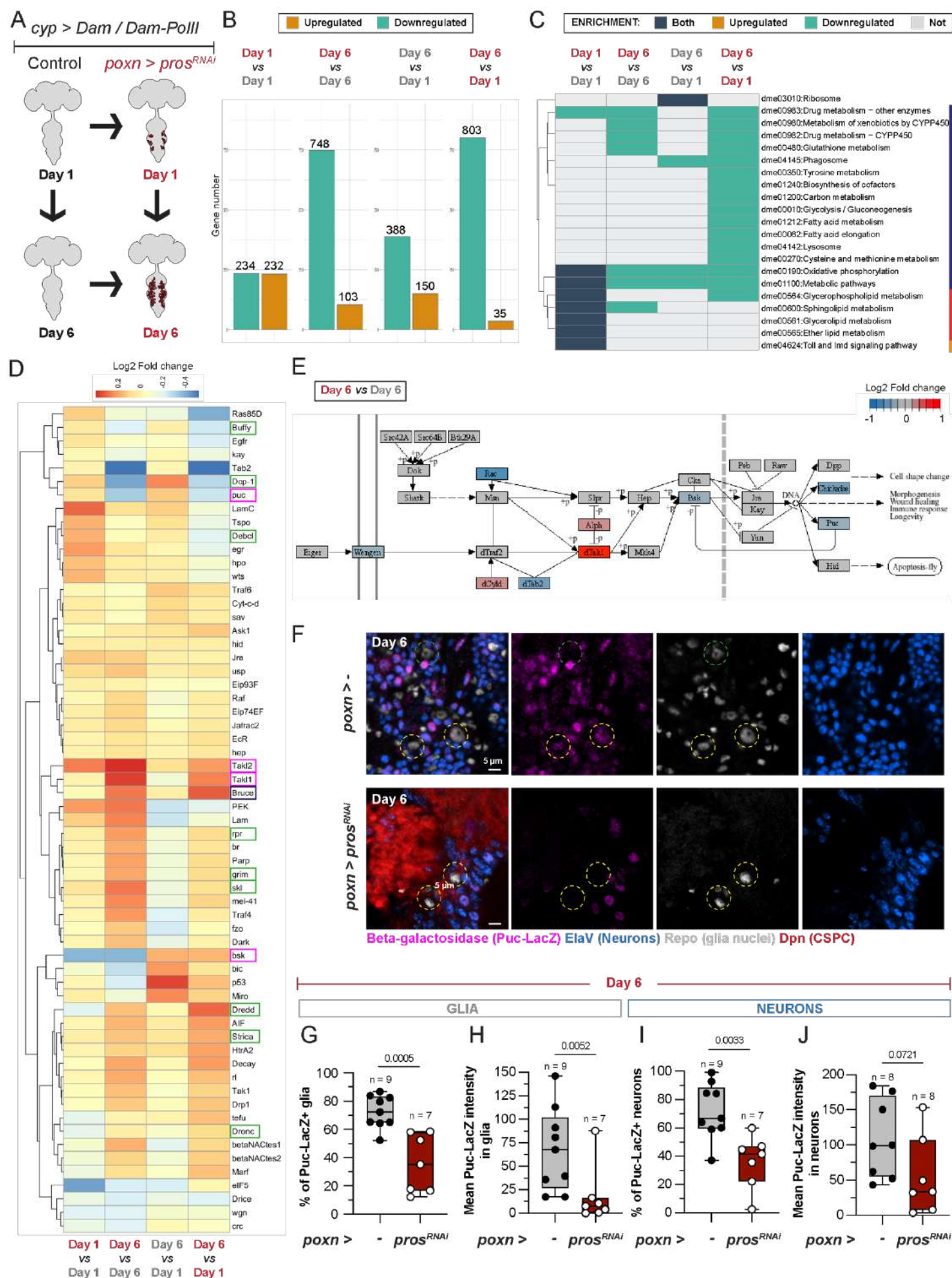**F** Beta-galactosidase (Puc-LacZ) ElaV (Neurons) Repo (glia nuclei) Dpn (CSPC)

1 **Figure 5. Cortex glia show a biphasic transcriptional response to tumour progression,**

2 **with an early specific signature shifting to global downregulation of core processes,**

3 **including the JNK pathway**

4 (**A**) Principle of the comparative Targeted DamID strategy. Either the Dam-PolII fusion, which

5 methylates around PolII binding sites, or the Dam only construct, which accounts for

6 background non-specific methylation, is specifically expressed in the CG under the control of

7 a specific enhancer and using the QF system *(cyp > Dam/Dam-PolII)*. Activation of their

8 expression is controlled through heatshock and induced either at day 1 or at day 6, 16 h before

9 dissection. Their combination with *poxn > -* or *poxn > pros^{RNAi}* allows the transcriptional

10 profiling of CG cells in control (non-tumour) and tumour conditions respectively, for two

11 timepoints. This produces four datasets in total. Control conditions at days 1 and 6 are coded in

12 black font (*poxn > -, cyp > Dam-PolII* normalized by *poxn > -, cyp > Dam*). Tumour conditions

13 at days 1 and 6 are coded in red font (*poxn > pros^{RNAi}, cyp > Dam-PolII* normalized by *poxn >*

14 *pros^{RNAi}, cyp > Dam*).

15 (**B**) Histograms showing the number of differentially expressed genes between the four

16 different conditions.

17 (**C**) KEGG pathway enrichment heatmap across the four conditions. The light and dark orange

18 lines indicate the specific early signature (day 1) of CG in tumour conditions, revealing an

19 immune (light orange) and a lipid metabolism (dark orange) components. The dark blue line

20 indicates the overall downregulation in several core metabolic pathways.

21 (**D**) Differential expression heatmap for genes of the KEGG apoptosis pathway. Fold change

22 scale is in Log2. Green boxes indicate genes of the core apoptotic cascade whose differential

23 expressions support its activation in CG cells upon tumour progression. Dark blue boxes

24 indicate genes of the core apoptotic cascade which are downregulated upon tumour progression.

25 Pink boxes indicate genes of the JNK pathway whose differential expressions support its

26 downregulation in CG cells upon tumour progression.

27 (**E**) Part of the map of the KEGG *Drosophila* MAPK signalling pathway (Entry dme04013)

28 with differential expression at day 6 between tumour and control conditions overlaid as shades

29 on the gene boxes. Basket (Bsk), the *Drosophila* JNK, and Puckered (Puc), an inhibitor of the

30 JNK pathway whose expression is positively controlled by pathway activation, are both

31 downregulated in tumour condition.

32 (**F**) Confocal images showing the expression of the *puc-lacZ* reporter (magenta, β-galactosidase

33 staining), whose expression is a readout of JNK pathway activation at day 6 of adulthood in

34 control (non tumour) and *pros^{poxn}* tumour conditions. Dashed yellow circles highlight *puc*

35   expression in glial cells.

36   (**G**) Box plot of the percentage of glial cells positive for *puc-lacZ*/β-galactosidase (Puc⁺ Repo⁺

37   cells) at day 6 in control (non tumour) and tumour conditions. n = VNC. Mann-Whitney U test.

38   (**H**) Box plot of the mean intensity of *puc-lacZ* in glial cells positive for *puc-lacZ*/β-

39   galactosidase (Puc⁺ Repo⁺ cells, so excluding Repo⁺ cells with no detected β-galactosidase

40   signal) at day 6 in control (non tumour) and tumour conditions. n = VNC. Mann-Whitney U

41   test.

42   (**I**) Box plot of the percentage of neurons positive for *puc-lacZ*/β-galactosidase (Puc⁺ ElaV⁺

43   cells) at day 6 in control (non tumour) and tumour conditions. n = VNC. Unpaired Student t-

44   test.

45   (**J**) Box plot of the mean intensity of *puc-lacZ* in neurons positive for *puc-lacZ*/β-galactosidase

46   (Puc⁺ ElaV⁺ cells, so excluding ElaV⁺ cells with no detected β-galactosidase signal) at day 6 in

47   control (non tumour) and tumour conditions. n = VNC. Mann-Whitney U test.

48

49   For box plots, individual values are superimposed.

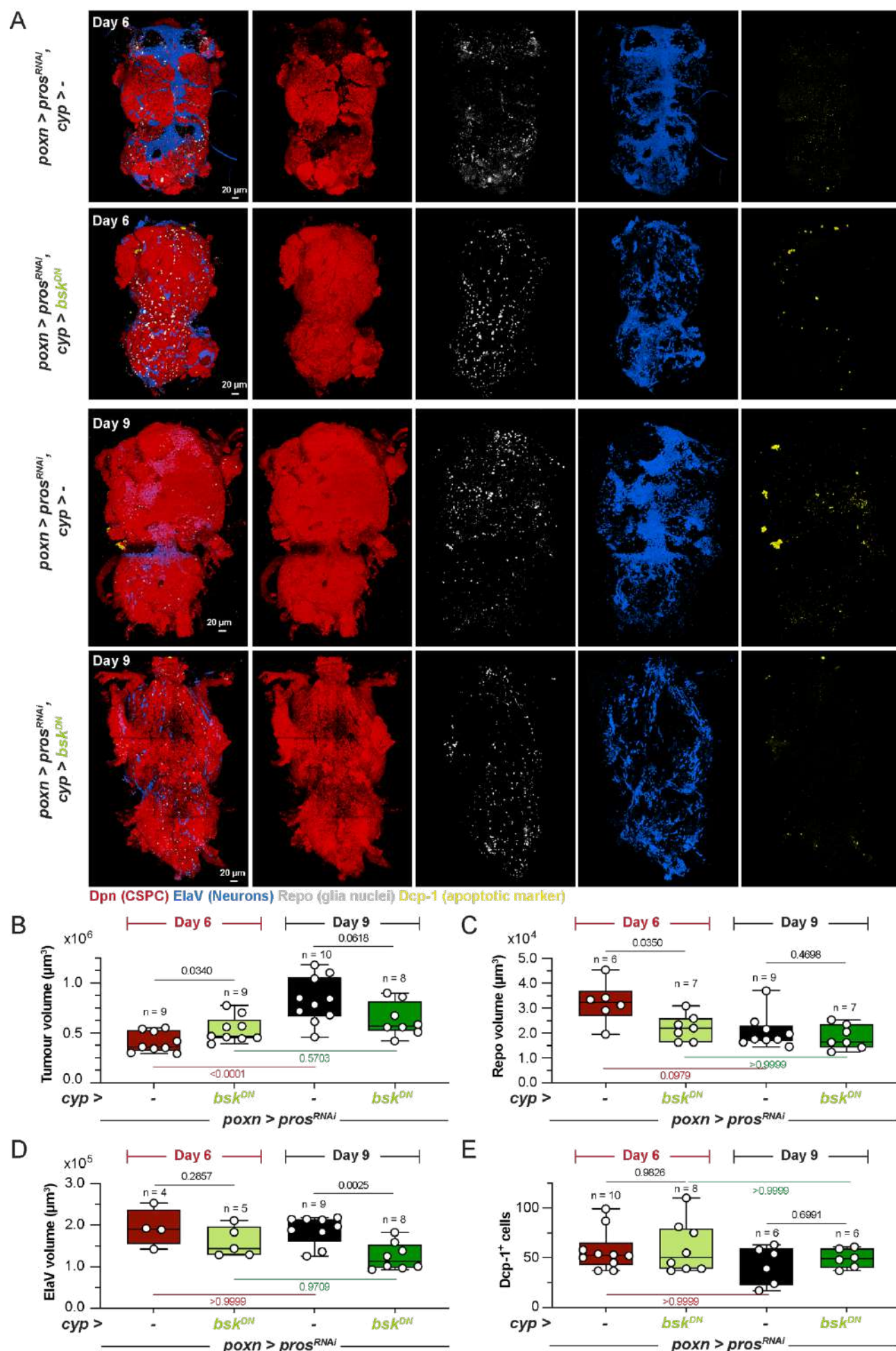50   See also Table S1 and Datasets S1 and S2.

Figure 6

Dpn (CSPC) ElaV (Neurons) Repo (glia nuclei) Dcp-1 (apoptotic marker)

14

1 **Figure 6. The JNK pathway in CG first hinders then supports tumour growth while**

2 **protecting neurons from apoptosis**

3 (**A**) 3D reconstruction of confocal images showing whole VNCs stained for tumour (Dpn, red),

4 glial cells (Repo, gray), neurons (ElaV, blue) and apoptotic cells (Dcp-1, yellow) for control

5 tumours (*poxn > pros^{RNAi}, cyp > -*) and tumours in which a dominant negative form of Bsk has

6 been induced from day 0 in all CG cells (*poxn > pros^{RNAi}, cyp > bsk^{DN}*) at days 6 and 9 of

7 adulthood.

8 (**B**) Box plot of tumour (Dpn) volume for (*poxn > pros^{RNAi}, cyp > -*) and (*poxn > pros^{RNAi}, cyp*

9 *> bsk^{DN}*) at days 6 and 9 of adulthood. n = VNC. One-way ANOVA with with Tukey's multiple

10 comparisons test between days. Student's t-tests between control and *bsk^{DN}* conditions for each

11 day. One outlier was removed for (*poxn > pros^{RNAi}, cyp > bsk^{DN}*) at day 6.

12 (**C**) Box plot of glia (Repo) volume per VNC for (*poxn > pros^{RNAi}, cyp > -*) and (*poxn >*

13 *pros^{RNAi}, cyp > bsk^{DN}*) at days 6 and 9 of adulthood. n = VNC. Kruskal-Wallis with with Dunn's

14 multiple comparisons test between days. Mann-Whitney U tests between control and *bsk^{DN}*

15 conditions for each day.

16 (**D**) Box plot of neuron (ElaV) volume per VNC for (*poxn > pros^{RNAi}, cyp > -*) and (*poxn >*

17 *pros^{RNAi}, cyp > bsk^{DN}*) at days 6 and 9 of adulthood. n = VNC. Kruskal Wallis with Dunn's

18 multiple comparisons test between days. Mann-Whitney U tests between control and *bsk^{DN}*

19 conditions for each day.

20 (**E**) Box plot of apoptotic cell (Dcp-1) numbers per VNC for (*poxn > pros^{RNAi}, cyp > -*) and

21 (*poxn > pros^{RNAi}, cyp > bsk^{DN}*) at days 6 and 9 of adulthood. n = VNC. Kruskal Wallis with

22 with Dunn's multiple comparisons test between days. Mann-Whitney U tests between control

23 and *bsk^{DN}* conditions for each day.

24

25 For box plots, individual values are superimposed.
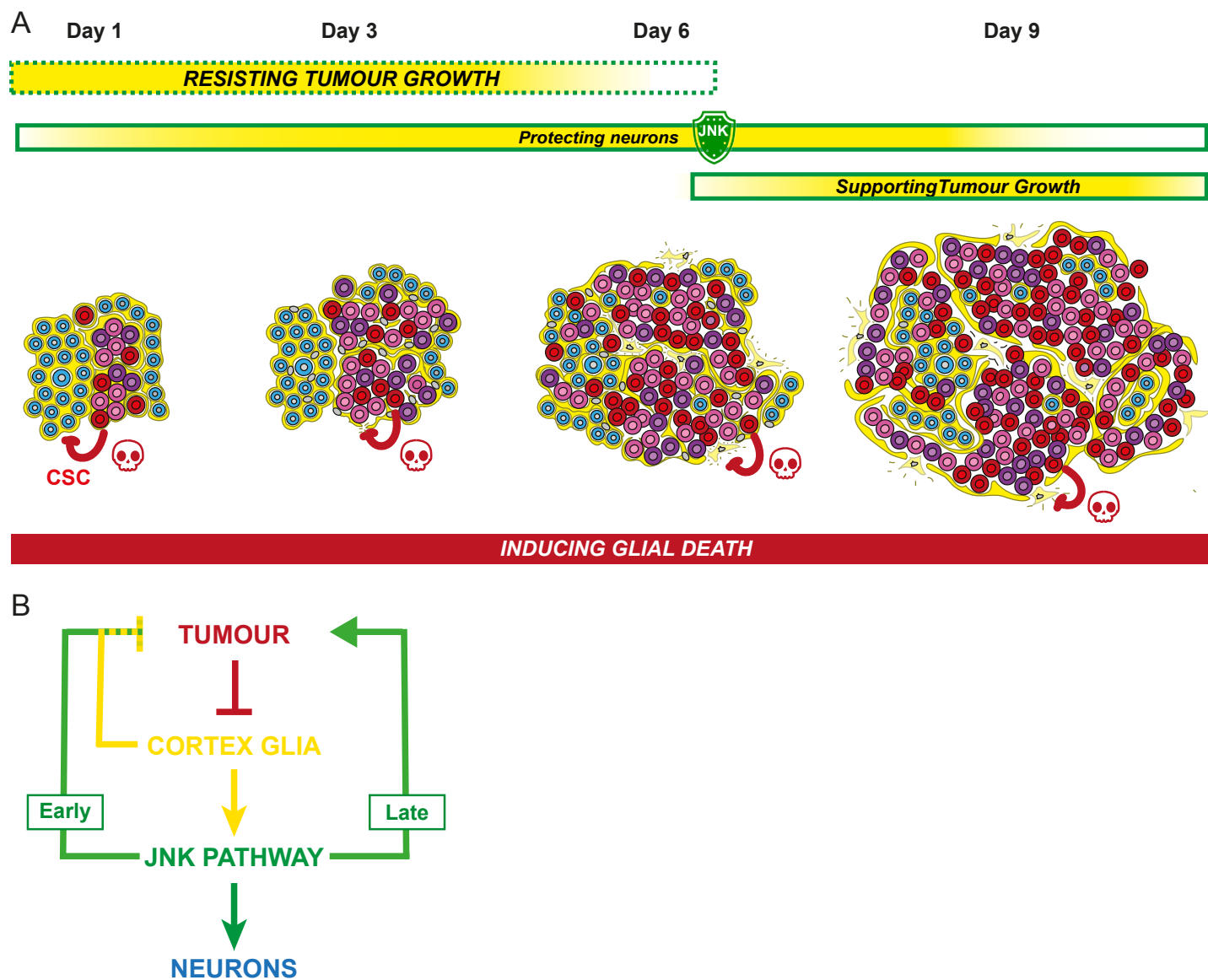
26 See also Tables S1 and S2.

Figure 7

Figure 7. Dynamics of interplay between cortex glia cells and tumour progression

(A) *pros^{poxn}* tumours, driven by CSCs (red), and whose bulk is made of CPCs (pink and purple) grow extensively in a TME made of CG cells (yellow) and neurons (blue) between day 1 and day 9 of adulthood. Tumour growth triggers the remodelling of CG membranes, which infiltrate within each tumour mass while keeping the original enwrapping at its boundary. In addition, CSC-driven tumour progression induces apoptosis of the CG cells (red arrows), what decreases the density of CG infiltration. This creates a dynamic balance: CG death favours tumour growth, while CG presence provides resistance to such growth. Early resistance relies in part on intrinsic, pre-existing JNK signalling (green coded) in the CG, a pathway which also protects neurons from death. Yet other mechanisms, regulated by the JNK pathway, also exist in the CG to play an opposite supportive role for tumour growth in later phases -possibly by preventing the collapse of the host tissue and its diverse support functions.

(B) Tumour growth leads to CG apoptosis, a cell loss which results in the overall decrease of JNK signalling normally active in the CG cells. Initially, intrinsic JNK activity provide some resistance to tumour growth, and its downregulation further favours tumour growth, setting up an amplifying loop (Early). However, over time JNK signalling becomes essential for tumour support and its loss in CG is detrimental to tumour progression, which starts to stall (Late). The latter phase coincides with neuronal loss, supporting a neuroprotective role of the JNK pathway in CG.